PHYSICAL REVIEW B VOLUME 18, NUMBER 12 15 DECEMBER 1978

Self-consistent augmented-plane-wave electronic-structure calculations for the $A15$ compounds V_3X and Nb_3X, X = Al, Ga, Si, Ge, and Sn

B. M. Klein, L. L. Boyer, and D. A. Papaconstantopoulos
Naval Research Laboratory, Washington, D.C. 20375

L. F. Mattheiss
Bell Telephone Laboratories, Murray Hill, New Jersey 07974

(Received 5 July 1978)

We have performed self-consistent (SC) band-structure calculations for the $A15$ compounds V_3X and Nb_3X, X = Al, Ga, Si, Ge, and Sn, using the augmented-plane-wave (APW) method. Relativistic effects (except the spin-orbit interaction) have been included in each SC cycle, along with corrections to the usual muffin-tin approximation. The latter apply the APW wave functions outside of the muffin-tin spheres to compute the interstitial charge densities and potentials. The resulting interstitial potential has full cubic symmetry (no spherical averaging), although a spherically averaged muffin-tin form is retained inside the spheres. The final SC potentials were used to generate energies and wave functions on a cubic mesh of 35 $\vec{k}$ points in 1/48th of the Brillouin zone. These results were interpolated onto a finer mesh of 969 $\vec{k}$ points using a symmetrized Fourier method; the densities of states (DOS), $N(E)$, were determined using tetrahedral integration. These accurate interpolation methods allow us to determine the DOS on a fine energy scale (± 3 mRy) around the Fermi level E_F, where we find large variations for the compounds V_3Ga, V_3Si, and Nb_3Sn. This correlates well with the fact that these compounds have high superconducting transition temperatures (T_c) and anomalous electronically derived properties. The energy bands of the $A15$ materials exhibit significant variations even amongst the isoelectronic compounds, both as to band shapes and positions of E_F. All compounds possess very flat bands that evolve from the Γ_{12} state near E_F and give rise to the sharp peaks in $N(E)$. For V_3Ga, V_3Si, and Nb_3Sn, E_F falls within several mRy of Γ_{12} so that these flat bands are responsible for the sharp structure in $N(E)$ at E_F. We find that Nb_3Ge and Nb_3Si have relatively low values of $N(E_F)$, which suggests that the high T_c's observed in films of the former and predicted for the latter are due to unusual mechanisms. We argue that the high T_c in Nb_3Ge may be related to soft-phonon modes, disorder, or impurities in the films. Soft x-ray-emission calculations (including matrix elements) of K and L spectra for the vanadium compounds are shown to compare well with experiment. Calculated x-ray photoemission spectra for V_3Si, Nb_3Ge, and Nb_3Sn are also in reasonable agreement with the available data.

I. INTRODUCTION

The A-15 compounds include materials having the highest superconducting transition temperatures (T_c) known. Many of the A-15's also exhibit unusual or anomalous low-temperature behavior of electronically derived properties such as elastic constants, Knight shifts, electrical resistivity, and magnetic susceptibility. In addition two of the high-T_c members of the A-15 family, V_3Si (T_c = 17 °K) and Nb_3Sn (T_c = 18 °K), have martensitic cubic-to-tetragonal structural phase transitions as the temperature is lowered to T_m, which is somewhat above T_c. There is some less definitive evidence for structural transitions in V_3Ga and Nb_3Al. As a result of these unusual properties of the A-15's, and the desire to obtain even higher T_c materials through understanding their underlying physics, these compounds have been extensively studied both experimentally and theoretically over the past 20 years. Recent review articles by Testardi,[1] Weger and Goldberg,[2] and Izyumov and Kurmaev[3] describe all but the most recent work on these materials.

There have been several A-15 band-structure studies during the past 13 years. The first calculations were done by Mattheiss[4] in 1965 using the augmented-plane-wave (APW) method for several A-15 compounds, among which was V_3Ga included in our studies. These 1965 calculations were non-self-consistent, were done only at symmetry points in the Brillouin zone, and were relatively poorly converged (~30 mRy) due to computer limitations. Subsequent calculations by Mattheiss[5] in 1975 for V_3Si, V_3Ge, Nb_3Al, and Nb_3Sn had an order-of-magnitude better convergence, and, in addition, a linear combination of atomic orbitals (LCAO) interpolation was used to determine density-of-states [$N(E)$] curves, and other band-related quantities. Klein *et al.*[6,7] performed the first self-consistent APW calculation for V_3Si using techniques similar to those reported here. Jarlborg and Arbman[8] have done linear-muffin-tin-orbital (LMTO) band-structure calculations for several A-15 compounds. Weger, Goldberg, and Barak[2,9-11] have carried out tight-binding calculations for the A-15's, fitting their tight-binding pa-

rameters to Mattheiss' earlier APW results, and then empirically adjusting selected parameters to correct for what they believe are limitations of the muffin-tin APW method. Klein *et al.*[12] have recently reported self-consistent APW band-structure results for V_3Ga.

The present work involves *ab initio* self-consistent APW calculations of the band structures and densities of states of ten different A-15 compounds: V_3X and Nb_3X, X=Al, Ga, Si, Ge, and Sn. These include both high- and low-T_c compounds with valence electron per atom ratios of 4.5 and 4.75. By studying a variety of A-15's using the same band-structure formalism, we hope to obtain a coherent and consistent picture of the properties of these materials.

In 1961 Clogston and Jaccarino[13] suggested that the unusual temperature dependences observed in the properties of A-15 materials could be explained by the existence of sharply peaked structure in the electronic density of states near the Fermi energy E_F. Weger[14] observed that the chainlike structure of the A atoms in the A_3B A-15 compounds could produce a very narrow one-dimensional-like d-band structure which might give such sharp peaks. Subsequently $N(E)$ models by Labbé and Friedel[15] and Cohen *et al.*[16] were applied successfully to obtain detailed quantitative interpretations of the electronic properties of these materials. The former model has an $N(E)$ singularity of the form $(E-E_F)^{-1/2}$ while the latter model has a step discontinuity at E_F. More recently, symmetry-based models by Gor'kov,[17] Lee *et al.*,[18] and Bhatt[19] have also been successful. One of the major results of the present work is that such sharply peaked $N(E)$ structure follows directly from our first-principles band-structure calculations. Furthermore, the details of the A-15 electronic structure in the present work do not justify the basic assumptions of any of the proposed models. It is our view that these models merely parametrize the sharp density-of-states structure which occurs naturally in first-principles calculations.

Testardi[1,20] has proposed a theory of the A-15 materials which emphasizes anharmonicity in these compounds rather than the purely electronic instabilities (resulting from the peaked density of states). Although the electronic structure (energies and wave functions) are a key ingredient in any theoretical treatment of phonons or anharmonicity, we are not at the stage where our present results for the A-15's can be used in this type of analysis.

This paper will present and discuss the energy bands and $N(E)$ results for ten A-15 compounds, along with a comparison of theoretical and experimental soft-x-ray emission and x-ray photoelectron spectroscopy (XPS) spectra for a number of these materials. Subsequent papers will deal with predicted Fermi surfaces, electron-phonon interactions, detailed analysis of the density of states near E_F, and electronic charge densities.

The remaining sections in this paper are as follows: Sec. II discusses the band-structure and density-of-states techniques that we have used; in Sec. III we discuss the calculated energy bands and densities of states, including comparisons with previous band-structure work; in Sec. IV we compare calculated and measured x-ray and XPS spectra.

II. BAND-STRUCTURE METHODOLOGY

Our band-structure calculations follow the symmetrized APW method as discussed by Mattheiss, Wood, and Switendick,[21] with some modifications for including self-consistency, relativistic effects, corrections to the muffin-tin (MT) approximation, and some additional computer code modifications which we discuss below.

The A-15 crystal structure is cubic with two A_3B formula units per unit cell (see Fig. 1). The six A atoms in the unit cell lie in pairs on the cube faces and the two B atoms occupy a body-centered lattice. The maximum possible APW radii for nonoverlapping spheres are $R_A=\frac{1}{4}a$ and $R_B=\frac{1}{4}(\sqrt{5}-1)a$, with a being the cubic lattice constant. This choice of radii leads to 64% of the cell volume being enclosed inside the APW spheres. In each of the present calculations we have chosen $R_B=R_A=\frac{1}{4}a$ such that the B-atom APW radius is decreased by 19% from its maximum value. This choice of R_B reduces (by 12%) the total volume inside the APW spheres but has the advantage of increasing the volume of the interstitial region where a fully nonspherical potential is used (see below). There is no loss of convergence with this choice of R_B, since this is governed by the A-atom (V or Nb) valence-conduction d states for which $R_A=R_A(\max)$ has been used.[21] Table I lists the lattice constants and APW sphere radii that we have used.

A. Starting configurations

All of our calculations begin with starting MT spherical charge densities that are obtained by overlapping atomic spherical charge densities from five neighboring shells of atoms. These atomic charge densities are obtained from the relativistic Hartree-Fock-Slater atomic-structure code of Liberman, Cromer, and Waber,[22] suitably modified for the different local exchange approximations that we have used (see below). From the MT charge densities the starting Coulomb and exchange potentials are formed using standard techniques.[23,24]

We have divided the eigenstates of these com-

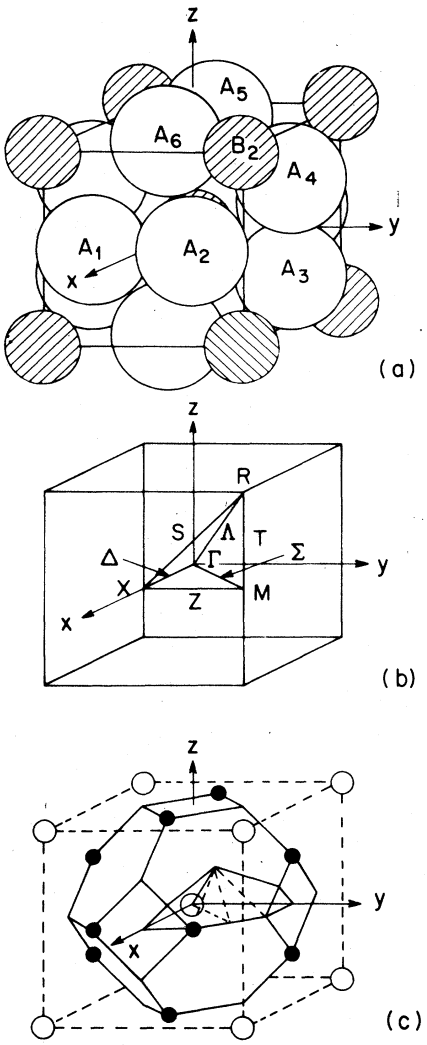

FIG. 1. (a) Primitive unit cell for A-15 compounds. (b) Brillouin zone for the simple cubic Bravais lattice. (c) Symmetry of the irreducible wedge representing $\frac{1}{48}$ of the unit cell.

pounds into three groups: core, semicore, and valence-conduction states. Table I shows this division for the A-15 compounds for which we have performed calculations. The core states lie deep in energy and have negligible bandwidths, so that we treat them self-consistently in an "atomiclike" approach. That is, the eigenvalues and wave functions of these states are calculated using the atomic-structure code,[22] but with the *crystal* MT potential as input.

The semicore states, defined in Table I, have relatively narrow bandwidths of less than 100 mRy for the A-atom s and p semicore, and ~3 mRy for the B-atom semicore. The charge in the APW spheres is 95% or more for these states. The strongly localized nature of these semicore states allows us to calculate these eigenstates on a rather course mesh in $\vec{k}$ space (see below).

The valence-conduction band states are formed initially from A-atom s and d orbitals, and B-atom s and p orbitals as shown in Table I. As we will discuss, these states are calculated on a finer $\vec{k}$-space mesh than the semicore states.

Finally note that for V_3Al the V $3s$ states were included in the core. This was done because of the overlap in energy between these states and the very narrow Al $2p$ band (~1 mRy bandwidth) which was also included in the core. Although this V $3s$ band had a bandwidth of ~20 mRy, the aforementioned overlap made it very inconvenient for us to include it in the semicore due to the nature of our computer codes. We believe that this change will have a negligible effect on our self-consistent (SC) V_3Al valence-conduction states.

B. Relativistic effects

Our calculations are carried out using a relativistic modification to the APW method which neglects spin-orbit coupling.[25] In this approach the terms corresponding to the spin-orbit interaction are effectively dropped from the Hamiltonian so that spin and orbital angular momenta remain good quantum numbers, the relativistic APW equations are significantly simplified over the fully relativistic case, and the symmetrization proceeds using single rather than double groups. The approach we have used is that of Koelling and Harmon[25] which avoids the "double-asymptote" problem that arises in the method of Mattheiss.[26] We have found that in the valence-band energy range, away from asymptotes, both methods give nearly identical energies and wave functions; the energy differences are 0.5 mRy or less for the cases we checked. However, the Koelling-Harmon approach is computationally much more convenient in the semicore and conduction-band energy ranges due to the presence of asymptotes there. Our neglect of spin-orbit coupling is probably not very serious (except possibly for details of the Fermi surface), especially for those states near the Fermi energy which are strongly dominated by V or Nb d orbitals, given the fact that these elements are of relatively low atomic number. A full quantitative assessment of the effects of the spin-orbit interaction will have to await future work. The core eigenstates were determined using the crystal muffin-tin potentials and the full Dirac-Slater Hamiltonian which includes spin-orbit coupling.[22]

C. Exchange approximations

The main body of our calculations were done using the local density functional approximation

TABLE I. Lattice constants (a), muffin-tin radii (R_A and R_B), configurations of the core and semicore states, and the starting open-shell configurations used to generate the initial potentials for the A-15 materials.

A_3B	a (Å)	$R_A=R_B$ (a.u.)	Core configuration $A(B)$	Semicore configuration $A(B)$	Starting open-shell configuration $A(B)$
V_3Al	4.830	2.282	Ne + $3s^2$(Ne)	$3p^6(\cdots)$	$3d^3 4s^1(3s^2 3p^1)$
V_3Ga	4.818	2.276	Ne(Ne)	$3s^2 3p^6(3d^{10})$	$3d^3 4s^1(4s^2 4p^1)$
V_3Si	4.722	2.231	Ne(Ne)	$3s^2 3p^6(\cdots)$	$3d^3 4s^1(3s^2 3p^2)$
V_3Ge	4.769	2.253	Ne(Ne)	$3s^2 3p^6(4d^{10})$	$3d^3 4s^1(4s^2 4p^2)$
V_3Sn	4.984	2.355	Ne(Kr)	$3s^2 3p^6(5d^{10})$	$3d^3 4s^1(5s^2 5p^2)$
Nb_3Al	5.187	2.451	Ar(Ne)	$4s^2 4p^6(\cdots)$	$4d^4 5s^1(3s^2 3p^1)$
Nb_3Ga	5.171	2.443	Ar(Ne)	$4s^2 4p^6(3d^{10})$	$4d^4 5s^1(4s^2 4p^1)$
Nb_3Si	5.030	2.376	Ar(Ne)	$4s^2 4p^6(\cdots)$	$4d^4 5s^1(3s^2 3p^2)$
	5.100	2.409	Ar(Ne)	$4s^2 4p^6(\cdots)$	$4d^4 5s^1(3s^2 3p^2)$
	5.200	2.457	Ar(Ne)	$4s^2 4p^6(\cdots)$	$4d^4 5s^1(3s^2 3p^2)$
Nb_3Ge	5.160	2.438	Ar(Ne)	$4s^2 4p^6(4d^{10})$	$4d^4 5s^1(4s^2 4p^2)$
Nb_3Sn	5.282	2.495	Ar(Kr)	$4s^2 4p^6(5d^{10})$	$4d^4 5s^1(5s^2 5p^2)$

(LDA) of Hedin and Lundqvist[27] for both the MT and interstitial regions. The exceptions are additional calculations that we did for V_3Ga and Nb_3Ge using a statistical $\rho^{1/3}$ exchange with $\alpha=\frac{2}{3}$—known as the Kohn-Sham-Gaspar exchange approximation.[28,29] The latter was done to assess the effects of changes in the exchange approximation on the A-15 band structure and will be described subsequently in this paper.

D. Corrections to the Muffin-Tin approximation

Our band-structure calculations have included corrections to the muffin-tin approximation, following the ideas of Schlosser and Marcus,[30] DeCicco,[31] Rudge,[32] and Koelling *et al.*[33] These MT corrections remove the common approximation of treating the charge density and potential outside of the APW spheres (interstitial region) as constants—equal to the average values in this region. The remaining MT approximation, using spherically averaged charge densities and potentials inside the APW spheres, has been retained. This overall approach is known as the warped muffin-tin (WMT) approximation.[34]

The detailed method that we have used closely follows the work of Refs. 32 and 33, although additional complications result from the fact that the A-15 crystal structure has a nonsymmorphic space group. Rudge[32] has shown how the use of symmetrized APW's may be handled within the framework of the WMT approach for symmorphic space groups; his techniques are readily extended to the nonsymmorphic case, although the algebra and computer programs become considerably more complex. Here we will briefly outline the methods that we have followed, using the case of unsymmetrized APW's. We refer the reader to Rudge's[32] paper for a discussion of the relevant group-theoretic modifications.

In the APW method the wave function in the interstitial region is given by

$$\psi_{\vec{k},n}(\vec{r}) = \sum_{\vec{G}} v_n(\vec{k}+\vec{G}) e^{i(\vec{k}+\vec{G})\cdot\vec{r}} \tag{1}$$

with $\vec{G}$ a reciprocal-lattice vector, $\vec{k}$ a vector in the irreducible Brillouin zone (IBZ), and n a band index. If we define the total interstitial potential to be $V_I(\vec{r})$ outside the APW spheres and zero inside, it is easy to see that the WMT correction to the $(\vec{G},\vec{G}')$ APW matrix element is $V_I(\vec{G}-\vec{G}')$. Therefore, all that is needed to include the WMT corrections in an APW calculation are the Fourier components of the WMT potential. Note that only the reciprocal-lattice vector components are required because of translational symmetry; and only those reciprocal-lattice vectors which are contained in Γ_1 are nonzero due to cubic symmetry.

Writing

$$V_I(\vec{r}) = V_I^{\text{coul}}(\vec{r}) + V_I^{\text{exch}}(\vec{r}) \tag{2}$$

for the Coulomb and exchange contributions, Rudge[32] shows how Eq. (1) can be used to generate

the Fourier components of the interstitial charge density, and using Poisson's equation, the values of $V_I^{\text{coul}}(\vec{G}-\vec{G}')$. Since $V_I^{\text{exch}}(\vec{r})$ is a nonlinear function of $\rho_I(\vec{r})$, generating it requires additional effort. There are two ways to proceed.

(a) DeCicco[31] and Rudge[32] suggest linearizing the real space-charge density,

$$[\rho_I(\vec{r})]^{1/3} \approx [\rho_I^{\text{av}}]^{1/3}[1+\tfrac{1}{3}\,\delta\rho_I(\vec{r})/\rho_I^{\text{av}}]\,,$$
$$\delta\rho_I(\vec{r}) \equiv \rho_I(\vec{r}) - \rho_I^{\text{av}}\,, \tag{3}$$

where ρ_I^{av} is the average charge density in the interstitial region. This linearization allows one to use the same techniques for obtaining $V_I^{\text{exch}}(\vec{G}-\vec{G}')$ as was used for the Coulombic part.

(b) Because the linearization of $\rho_I^{1/3}$ may be a serious approximation, we have used an improvement which follows the approach of Koelling *et al.*[33] In this approach one uses the APW values of $\rho_I(\vec{G})$ to obtain $\rho_I(\vec{r})$ by inverting the Fourier series. We thereby obtain $V_I^{\text{exch}}(\vec{r})$ directly, and finally determine $V_I^{\text{exch}}(\vec{G}-\vec{G}')$ by doing a least-squares Fourier fit, using a Monte Carlo sampling of $\vec{r}$ points in the interstitial region.[33] By sampling 800 $\vec{r}$ values, we have obtained fits such that the rms error is approximately 1% of the average value of the interstitial exchange potential. We find that the method of DeCicco[31] and Rudge[32] yields results for the exchange Fourier components which are nearly identical to the method of Koelling *et al.*[33] in the few cases where we have compared them. We therefore conclude that, for reasonably slowly varying $\rho_I(\vec{r})$ as are present in the A-15 materials, the two approaches give virtually equivalent band structures.

Both the Coulomb and exchange interstitial potentials are defined to have zero average values in the interstitial region. However, the Coulomb and exchange potentials within the APW spheres have arbitrary constants associated with them (for each inequivalent sphere). These constants have been determined by matching the spherical MT potential to the spherically averaged interstitial potential at each sphere radius in each SC cycle. Finally we note that the values of $V_I(\vec{G}-\vec{G}')$ from the previous cycle were used in generating the eigenstates for the following cycle.

All of our calculations were done using spherically averaged potentials inside the APW spheres. Although there will be some corrections to our results due to nonspherical potential components within the APW spheres, we do not feel that these corrections will be very large. A previous estimate by Mattheiss[5] showed that these nonspherical corrections produced eigenvalue shifts in V_3Si averaging ~3 mRy. Mattheiss made this estimate by doing WMT, non-SC, APW calculations for two different sets of V APW radii, one reduced by 10% from the other. The reduced APW radii transfers the largest nonspherical corrections into the interstitial region where a full general potential is used, so that comparing the energies for the two calculations gave the above-mentioned estimate of the nonspherical corrections inside the APW spheres.

E. Computational procedures for self-consistency

Since calculations for ten different A-15 compounds were being done, it was computationally convenient to calculate and store those parts of the APW matrices which depend on the structure alone. This procedure avoids having to repeat the time-consuming symmetrization procedures in each SC cycle for each compound. Mattheiss *et al.*[21] show how these structure-dependent terms may be stored and reused, subject to the condition that the APW radii keep the same ratios to the lattice constant for each calculation, as we have done. It is also possible to calculate once and store matrix quantities associated with the WMT aspect of the calculation; we have also done this.

In the SC procedure, eigenvalues and eigenfunctions are calculated for the semicore and valence-conduction states on a $\vec{k}$-space mesh, states are filled up to the Fermi level by occupying them with the appropriate number of electrons, and an occupied charge density is formed for the APW spheres and the interstitial region. The core charge density is obtained by using the crystal potential in the relativistic atomic-structure program,[22] and the WMT potentials are calculated using the procedure described above. To ensure stability we mixed 25% of the new charge density with 75% of the charge density from the previous cycle in forming the MT Coulombic and exchange potentials used in the following cycle. The WMT potential coefficients were not averaged, but were substituted in total into the next cycle. Convergence was considered to be achieved when the maximum change in valence eigenvalues between two successive cycles was less than 1 mRy, with the average eigenvalue change usually being less than 0.5 mRy. We found that 6–10 SC cycles were needed to reach convergence for these materials.

The first SC cycle in each calculation was performed without the warping correction. The output of the first cycle included the warped interstitial charge density, and each successive SC cycle had both input and output WMT charge densities and potentials.

F. $\vec{k}$-space meshes

Table II summarizes the $\vec{k}$-space meshes used in the different aspects of our calculations. For the

TABLE II. Summary of Brillouin-zone (BZ) meshes discussed in the text. IBZ denotes the irreducible BZ.

Points in IBZ	Points along ΓX (inclusive)	Points in BZ	No. of Tetrahedra[a] in IBZ
4	2	8	1
10	3	64	8
35	5	512	64
165	9	4096	512
969	17	32768	4096
6545	33	262144	32768

[a] Assumes all tetrahedra have the same volume, $\frac{1}{6}$ that of a subcube.

narrow bands of the semi-core states we used an iteration mesh of four $\vec{k}$ points in the IBZ. This mesh corresponds to eight points in the full BZ and includes the symmetry points $\Gamma(000)$, $X(010)$ $M(110)$, and $R(111)$, in units of π/a.

For the valence-conduction states a mesh of ten $\vec{k}$ points in the IBZ (64 $\vec{k}$ points in the full BZ) was used in the SC iterations. In addition to the four symmetry points, this mesh includes $\vec{k}$ points at the midpoints of the symmetry lines:

$$\Delta(0\alpha0),\ Z(\alpha10),\ \Sigma(\alpha\alpha0),\quad \Lambda(\alpha\alpha\alpha),\ S(\alpha1\alpha),\ T(11\alpha) \tag{4}$$

with $\alpha=\frac{1}{2}$.

After self-consistency was achieved, a final APW run was done on a mesh of 35 $\vec{k}$ points in the IBZ (512 $\vec{k}$ points in the full BZ) for determining the density of states (DOS) using techniques described in Sec. II G. This mesh includes the four symmetry points, three points along each symmetry line [$\alpha=\frac{1}{4},\frac{1}{2},\frac{3}{4}$ in Eq. (4)]; the twofold-symmetry points (in units of $\pi/4a$) (210), (211), (221), (310), (311), (320), (322), (331), (332), (421), (432), (431); and the general point (321).

Symmetrized APW's were constructed for these $\vec{k}$ points using the irreducible representations determined by Mattheiss[35] and the convergence criterion $|\vec{k}+\vec{G}|_{\max}=9(\pi/a)$ [see Eq. (1)]. This yielded eigenvalues converged to better than 1 mRy for all points except the general point, where some additional degradation of convergence was tolerated (~3 mRy) in the interest of making the computer runs shorter. The dimensions of the symmetrized APW matrices were: less than 100 for the symmetry points; ~100–185 for the symmetry lines; ~200 for the twofold points; and 300 for the general point.

Our computer codes ran ~12 min for each SC cycle and a total of ~90 min for each of the 35 $\vec{k}$-point mesh runs (five separate runs for ~40 bands). The computer used was a Texas Instruments Advanced Scientific computer.

G. Density of states calculations

For the determination of $N(E)$ and the site-angular-momentum decomposed density of states $N_s^l(E)$, we used a two-step procedure. We first interpolated the 35 $\vec{k}$-point mesh APW results onto a finer mesh in the IBZ using a symmetrized Fourier (SF) method.[36] We then used the tetrahedral method,[37-39] which involves linear interpolation, to perform the integrations necessary for obtaining the densities of states.

The SF method is designed to make the maximum use of the crystal symmetry, translational and rotational, in the choice of interpolating functions. Translational symmetry is built in through the use of a properly periodic Fourier series. Rotational symmetry leads to band crossings for $\vec{k}$ points on symmetry lines and planes. We account for this by first interpolating the band structure along symmetry lines using a one-dimensional Fourier series, and allowing bands of different symmetry to cross.

Next, these interpolated results are used, together with the compatibility relations, in the determination of the coefficients of two-dimensional Fourier series for the symmetry planes. In other words, the interpolated results along symmetry lines are used to force the interpolating function for the symmetry planes to have the proper behavior in the neighborhood of symmetry lines. In this way, sharp structure resulting from a symmetry-line band crossing, which is not allowed on the adjoining plane, is built into the two-dimensional Fourier series. Similarly the interpolated results along both symmetry lines and symmetry planes are used to determine the full three-dimensional Fourier series.

The $N(E)$ results shown in this paper were obtained by first using the SF method to interpolate from 35 to 969 $\vec{k}$ points in the IBZ, and then using the tetrahedral method[37-39] (4096 tetrahedra in the IBZ).

III. BAND-STRUCTURE AND DENSITY-OF-STATES RESULTS

Figures 2–14 show the energy bands and DOS for the A-15 compounds. The energy bands are plotted along the six symmetry directions shown using the $E(\vec{k})$ values from the interpolation scheme that we have described (35 APW input $\vec{k}$ points). The symmetry labels for the eigenvalues come directly from the computer storage, thus eliminating the chance of transcription errors.

The DOS shown in the lower part of Figs. 2–14

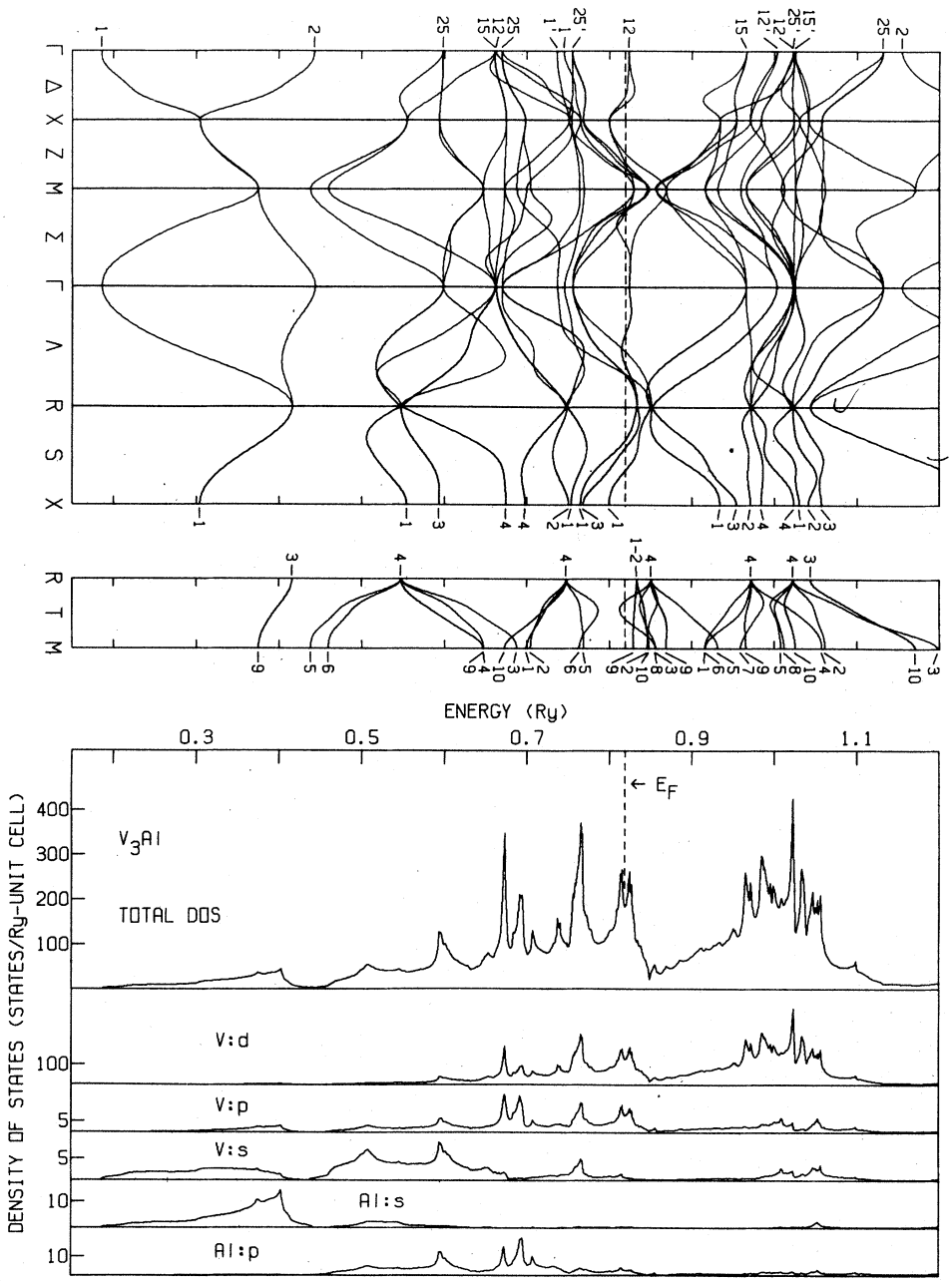

FIG. 2. Self-consistent energy bands and densities of states for V_3Al with the local density approximation exchange.

have been computed using the tetrahedral method in conjunction with the new interpolation scheme[36] we have described. The 35 point mesh eigenvalues have been interpolated onto a mesh of 969 $\vec{k}$ points in the IBZ, which corresponds to dividing the IBZ into 4096 tetrahedra (see Table II). By comparing DOS results for a 35 → 165 point mesh and a 35 → 6545 mesh interpolation (corresponding to 512 and 32 768 tetrahedra, respectively), we conclude that the DOS values from the 969 point mesh are accurate to ~1%. It should be noted that in all cases, the input to the tetrahedral program are interpolated energies and wave functions derived from the 35 point APW mesh. Consequently, the term "accuracy" is used here in a restricted sense that refers primarily to the validity of the linear interpolation that is utilized in the tetrahedral method.

The values of $N_s^l(E)$ shown in Figs. 2–14 were obtained by weighting the contributions to $N(E)$ with

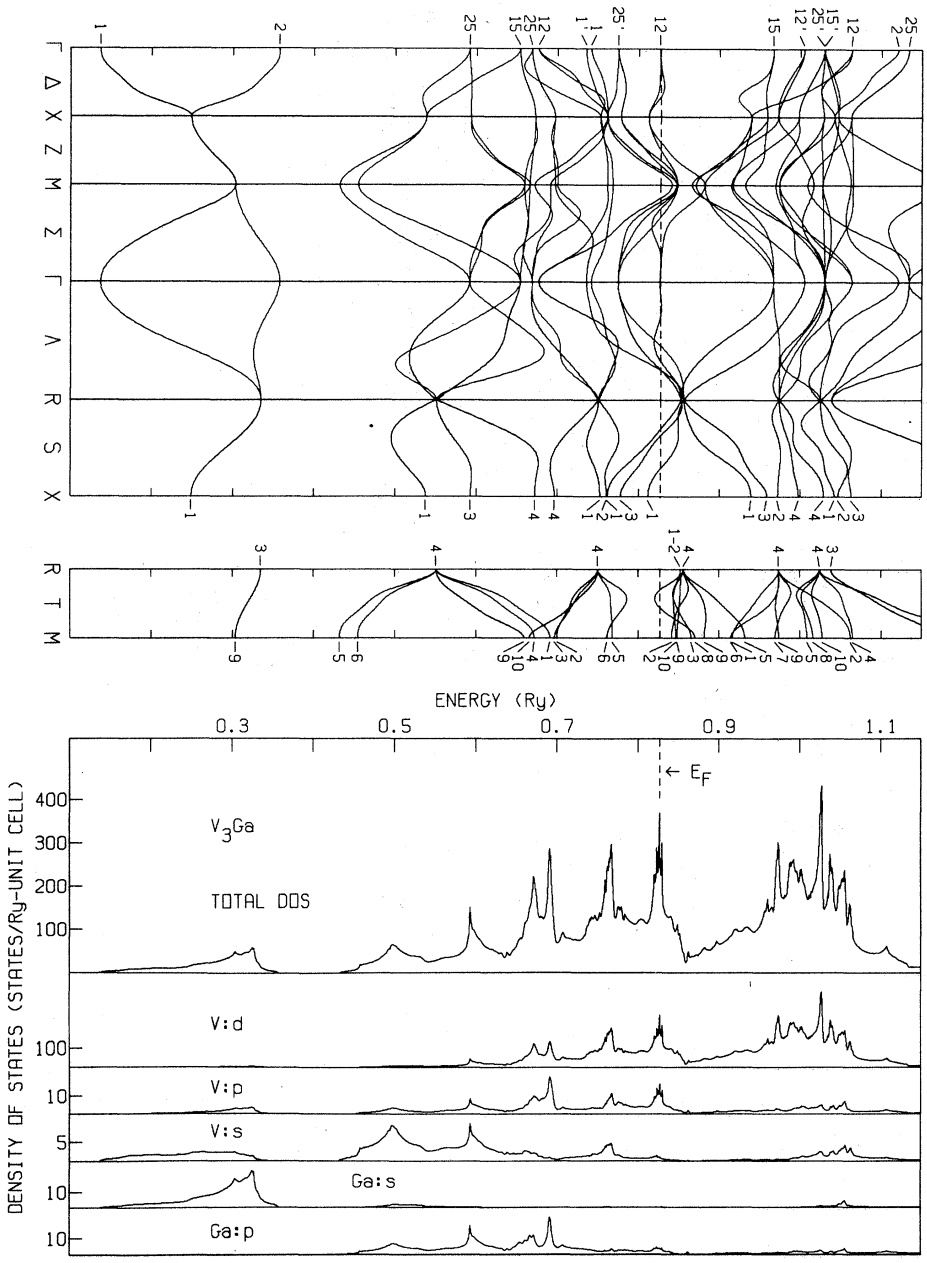

FIG. 3. Self-consistent energy bands and densities of states for V_3Ga with the local density approximation exchange.

the appropriate fractional charges that are contained within the six A-atom and two B-atom spheres with a given angular momentum l. These results do not include interstitial charge, so that

$$\sum_l \int_{E_{\text{bot}}}^{E_F} N^l_{A(B)}(E)\,dE$$

is the total valence charge in six A-atom (two B-atom) spheres. E_{bot} corresponds to the bottom of the valence bands. These $N^l_s(E)$ values are also calculated within the tetrahedral approach.

The Fermi energies shown are determined by integrating $N(E)$ to the energy where appropriate number of states are filled. Table III gives the values of $N(E_F)$ and $N^l_s(E_F)$ for our calculations. For those compounds with sharply peaked structure in $N(E)$ near E_F (V_3Ga, V_3Si, Nb_3Al, Nb_3Ga, and Nb_3Sn), there is an estimated uncertainty in $N(E_F)$ due to interpolation of ~10%, with the exception of V_3Ga. In this compound, even

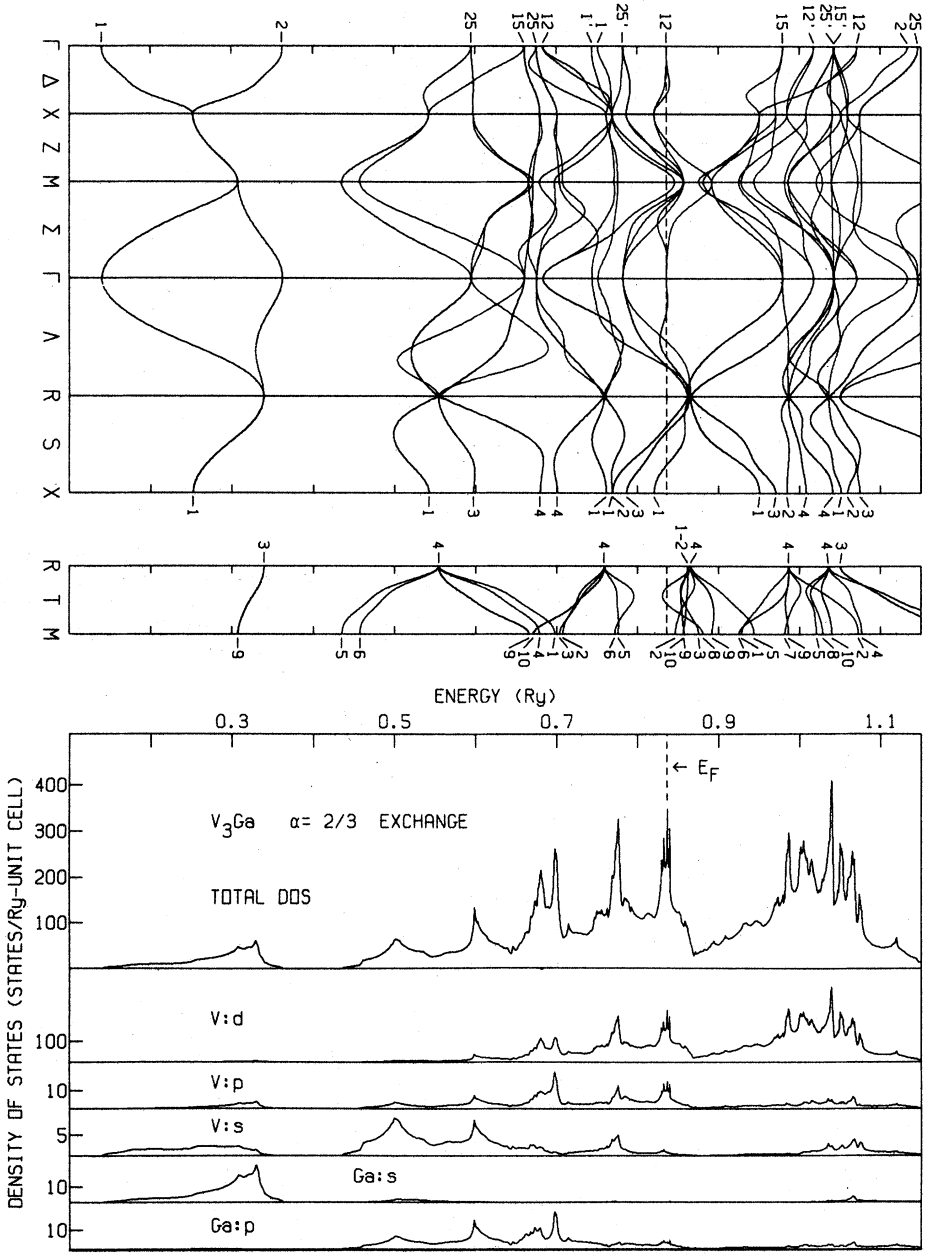

FIG. 4. Self-consistent energy bands and densities of states for V_3Ga with the $\alpha = \frac{2}{3}$ local exchange approximation.

though the calculations involving two different exchange approximations (Figs. 3 and 4) give band structures that are almost identical in appearance, the fine structure near E_F is so delicate that the $N(E_F)$ values differ by ~20% For the remaining compounds, where $N(E)$ is relatively flat around E_F, the values in Table III should be accurate to within a few percent.

A. General discussion of the energy bands

Some of the general features common to all of the band structures are the following.

(a) A low-lying (centered ≈0.5 Ry below E_F) pair of bands whose wave functions consist primarily of B-atom s-type oribtals. With the exception of V_3Al, these bands are separated by an energy gap

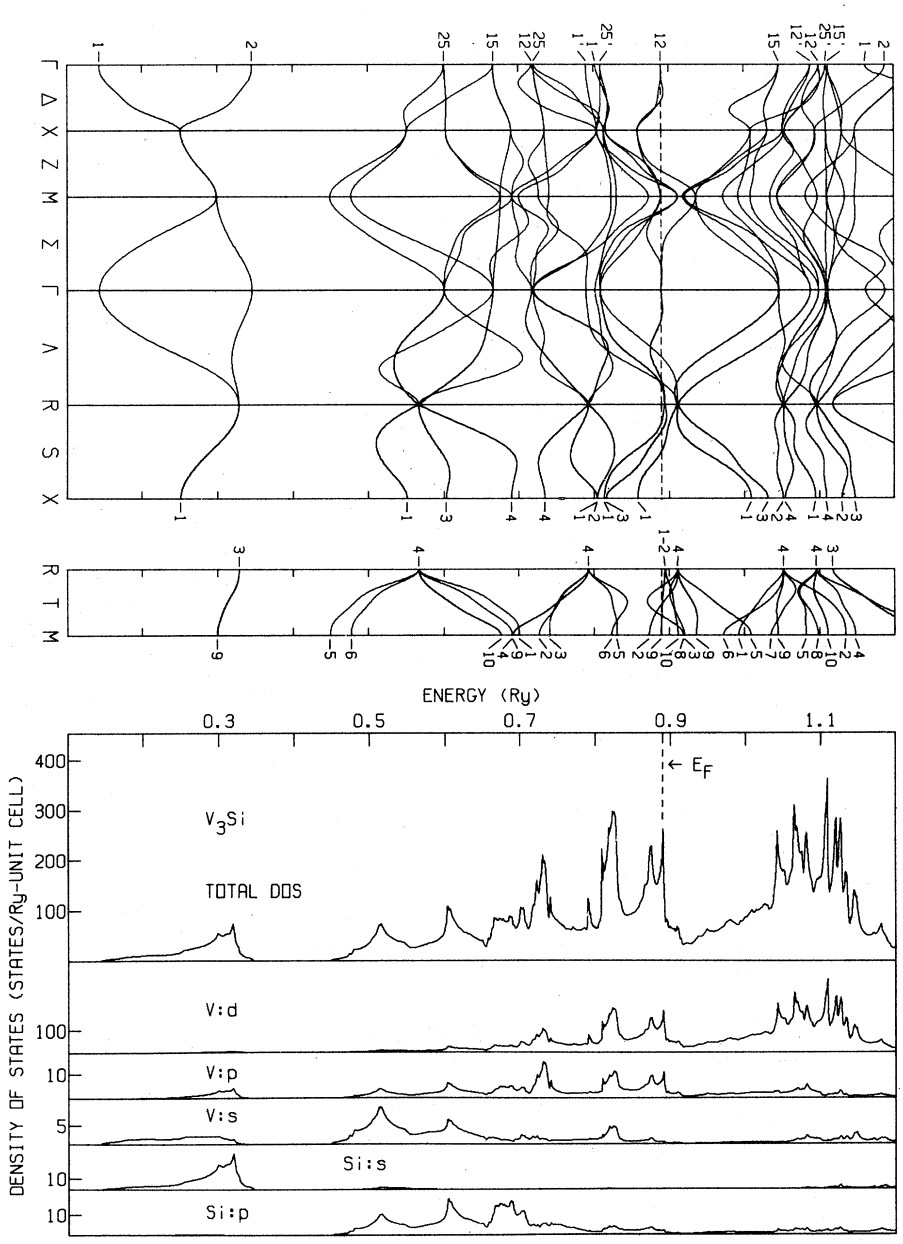

FIG. 5. Self-consistent energy bands and densities of states for V_3Si with the local density approximation exchange.

from the higher hybrid bands to be described. For the Nb compounds, these bands are systemically narrower and the $N(E)$ peak in this energy range is sharper than in the corresponding V compounds. This is apparently due to the larger lattice constants for the Nb compounds (see Table I) which results in a correspondingly smaller interaction between the s and p states of the A and B atoms.

(b) The next group of ~20 bands include a manifold of s-p-d hybrid states which extend from M_5 up to the Γ_{12} state which is consistently near E_F. The DOS show a number of peaks and valleys in this region corresponding to the particular locations of the critical points and the shapes of the bands. This energy-band complex can accomodate more than 30 electrons, and is dominated by the A-atom d-like wave functions, especially in the vicinity of E_F.

(c) Slightly above E_F, $N(E)$ systematically exhibits a minimum, above which a superposition of broad s-p bands and narrow A-atom antibonding d bands combine to give rise to more sharp struc-

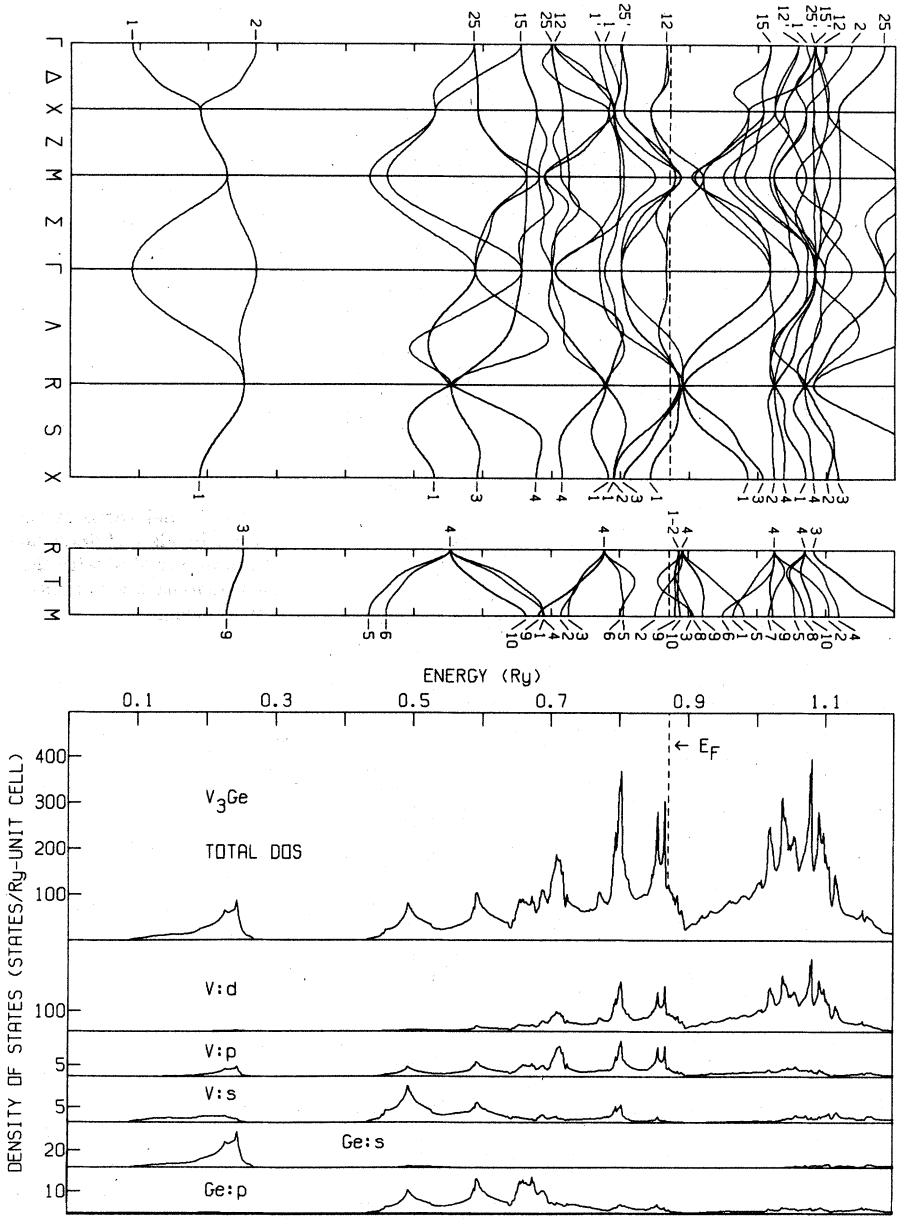

FIG. 6. Self-consistent energy bands and densities of states for V_3Ge with the local density approximation exchange.

ture in $N(E)$. The total range of energy shown in Figs. 2–14 includes a total of between 70–80 available electronic states per cell (35–40 bands).

B. Electronic structure near E_F

It is clear from Figs. 2–14 that many of the compounds have extremely sharp structure in $N(E)$ near E_F which arises either from very flat energy bands or band minima along the Σ and Λ directions. Among the high-T_c materials, Nb_3Ge and Nb_3Si are exceptions to this rule which we will discuss separately below.

The compounds V_3Ga (Figs. 3 and 4), V_3Si (Fig. 5), and Nb_3Sn (Fig. 14) stand out for their very flat bands at E_F along the Σ, Λ, and Δ directions around the Γ_{12} point. These materials are renowned, not only for their high-T_c values, but also for their anomalous low-temperature behavior which has been ascribed to just such a sharp $N(E)$ structure. In examining Figs. 3–5 and 14 by eye, it is clear that any quantitative interpretation is

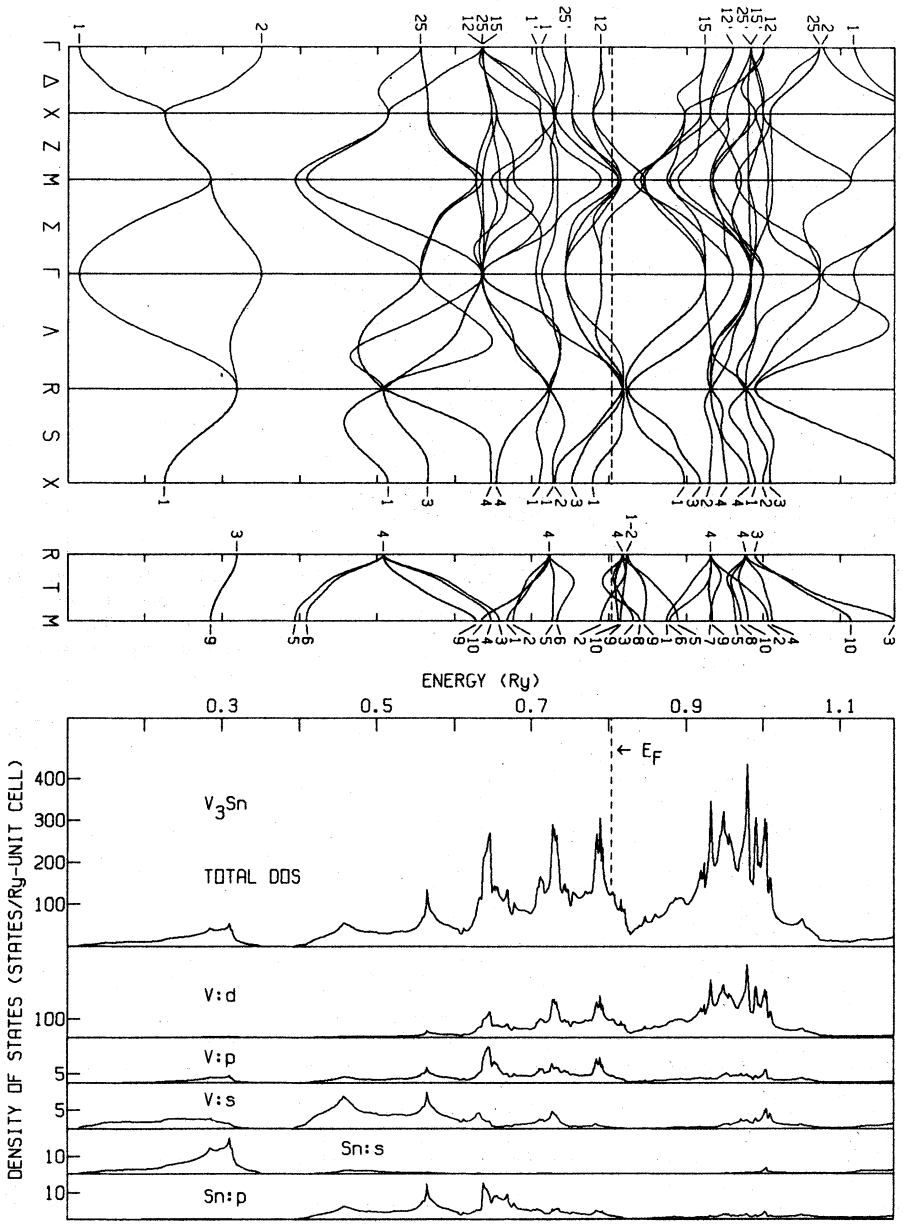

FIG. 7. Self-consistent energy bands and densities of states for V_3Sn with the local density approximation exchange.

limited by the "pen-width," so that we refer to Table IV where the *ab initio* APW eigenvalues corresponding to the states Δ_1, Δ_2, Σ_1, Σ_4, and Λ_3 (near E_F) are tabulated. From Table IV we see that significant fine structure on a scale of 1 mRy or less can certainly be anticipated from our APW results. We note that these qualitative conclusions are not sensitive to the exchange approximation (see Figs. 3 and 4 and the discussion in Sec. III C).

Figure 15 shows plots of $N(E)$ for Nb_3Sn and V_3Sn in a range ±3 mRy (~± 450°K) around E_F for each compound. The rather dramatic difference between $N(E)$ for these two isoelectronic materials is quite striking. For Nb_3Sn, $N(E)$ varies by ≈50% in a range of ≈±1 mRy around E_F, while $N(E)$ for V_3Sn is nearly constant. We have found equally abrupt variations in $N(E)$ near E_F in both V_3Si and V_3Ga; all three of these materials exhibit low-temperature anomalies. These rapid variations in $N(E)$ near E_F are of the right magnitude to explain the observed anomalies in elastic constants, susceptibilities, Knight shifts, etc.,[1-3] without any adjust-

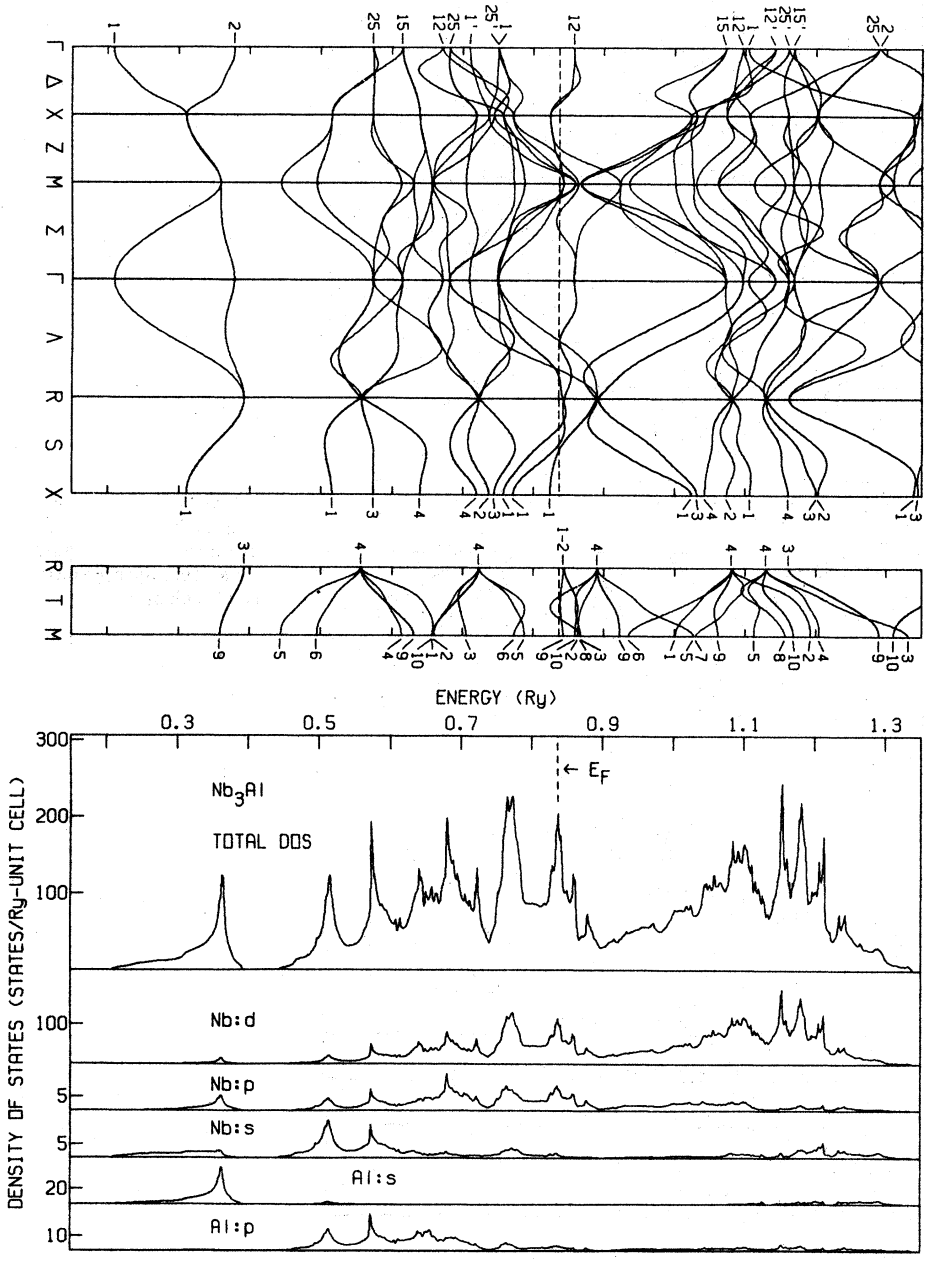

FIG. 8. Self-consistent energy bands and densities of states for Nb_3Al with the local density approximation exchange.

able parameters or model assumptions pertaining to the electronic structure. For the remaining A-15 compounds that we have considered, $N(E)$ varies by ~10% or less within ±3 mRy of E_F.

In attempting a quantitative study of such fine $N(E)$ structure, we are faced with two fundamental problems. The first is that our APW eigenvalues and eigenfunctions have an intrinsic convergence limitation that is governed by the size of the basis set. We estimate that within the APW approach that we are using the energies are converged to better than 1.0 mRy (~3 mRy for the general point). A second limitation results from our $\vec{k}$-space interpolation procedure, which starts with limited APW input data (35 point mesh energies and eigenfunctions), and then systematically generates intermediate values on higher-order meshes using the procedure which we described. The flexibility of this interpolation scheme will enable us to quantitatively assess the accuracy of the present $N(E)$

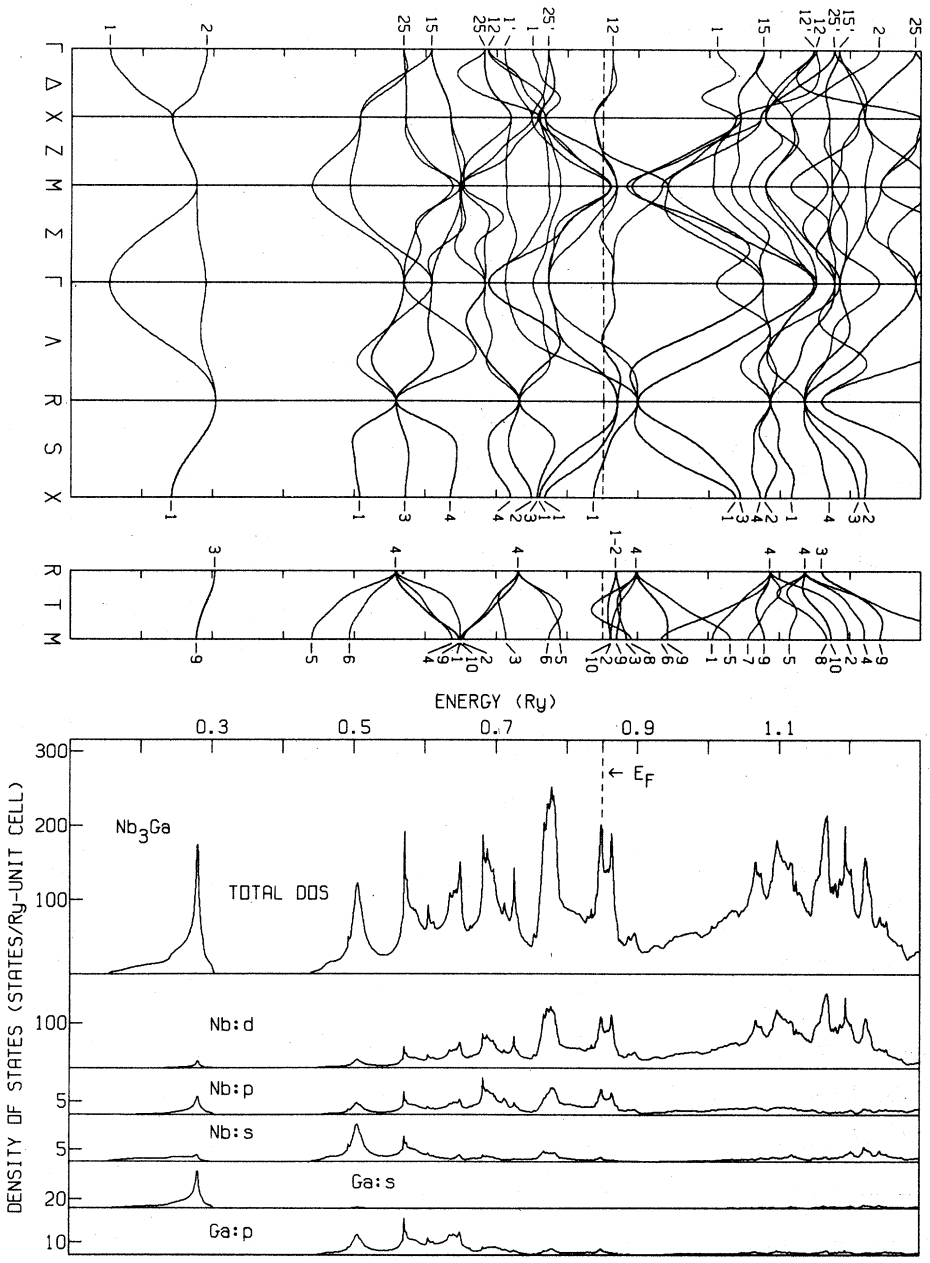

FIG. 9. Self-consistent energy bands and densities of states for Nb_3Ga with the local density approximation exchange.

results in future work. In such studies, we can input more first-principles APW data in the vicinity of E_F, so that these regions of very flat bands will be more accurately interpolated. The reader should bear in mind that $N(E)$ is determined by the slope of the bands which are likely to be more accurate than the absolute value of the eigenvalues.

An additional concern is the role of spin-orbit coupling, neglected in the present calculations, on the DOS fine structure. Fortunately the flat bands near E_F in V_3Ga, V_3Si, and Nb_3Sn (Γ_{12}-$\Sigma_{1,4}$ and Γ_{12}-Λ_3) are not spin-orbit-split at all at Γ. Spin-orbit splitting can occur along Λ (Λ_3 state), but this splitting is expected to be small near Γ_{12} where the bands are very flat. Spin-orbit coupling can shift the bands at Γ and along the Σ and Δ lines, but it will not further reduce their degeneracy. We conclude that spin-orbit effects are likely to be important for predicting an accurate representation of the Fermi surface in at least some of

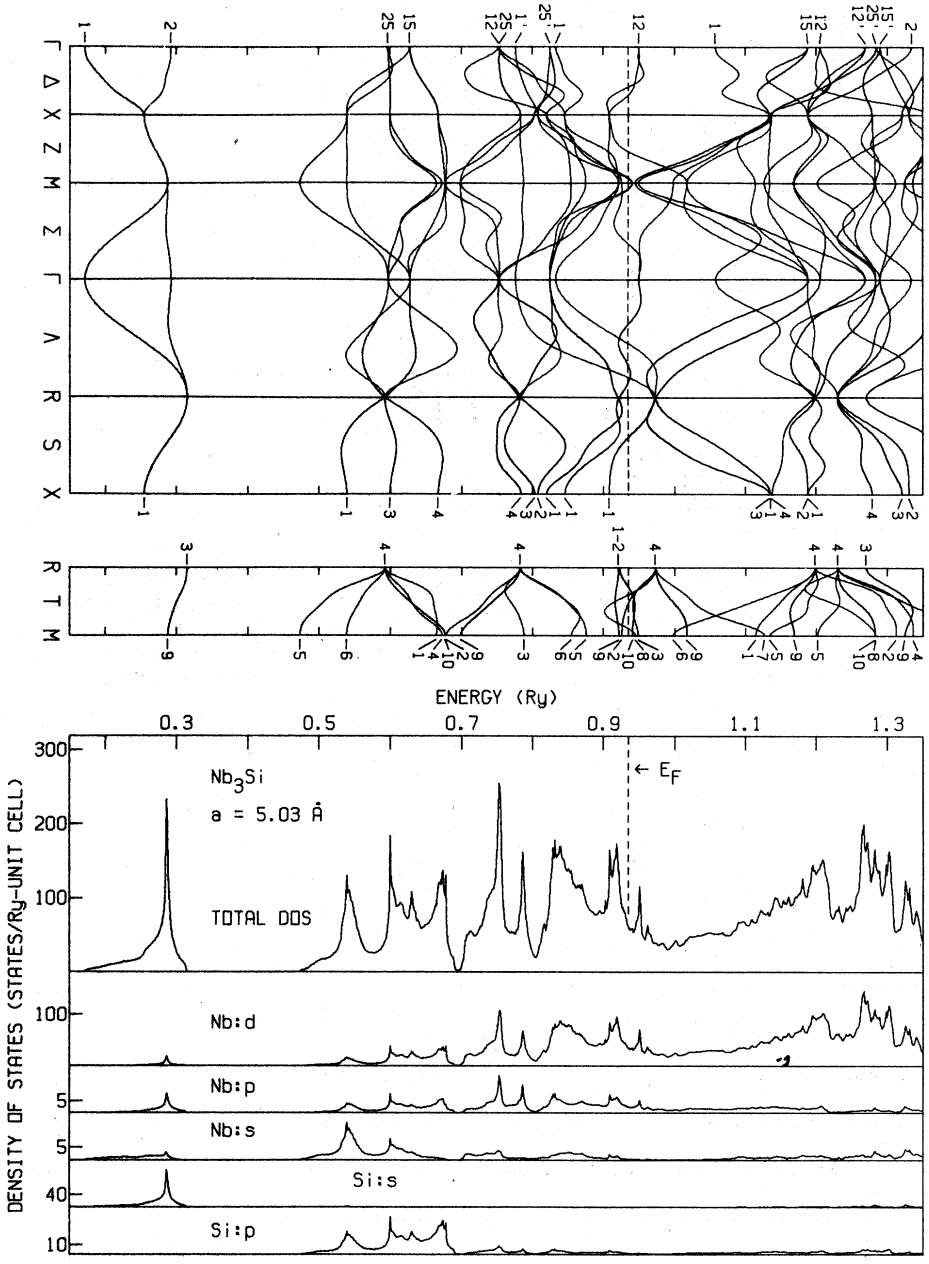

FIG. 10. Self-consistent energy bands and densities of states for Nb_3Si ($a = 5.03$ Å) with the local density approximation exchange.

the A-15 materials, particularly those compounds with heavy B atoms such as Nb_3Sn. This will be explored in subsequent publications.

C. Sensitivity of the band structures to the exchange approximations

A common concern in all band-structure calculations and their interpretation is the fact that approximations are made for treating exchange-correlation effects. In the present set of A-15 calculations, the majority of the work was performed using the local density approximation (LDA),[27] as it is widely agreed that this approach has the firmest theoretical foundation of all of the present one-electron approximations. Previous work that has been done on the bcc transition metals V and Nb (Ref. 40) showed that the band structures and Fermi surfaces have a quantitative dependence on the exchange potential used (~10% variation in Fer-

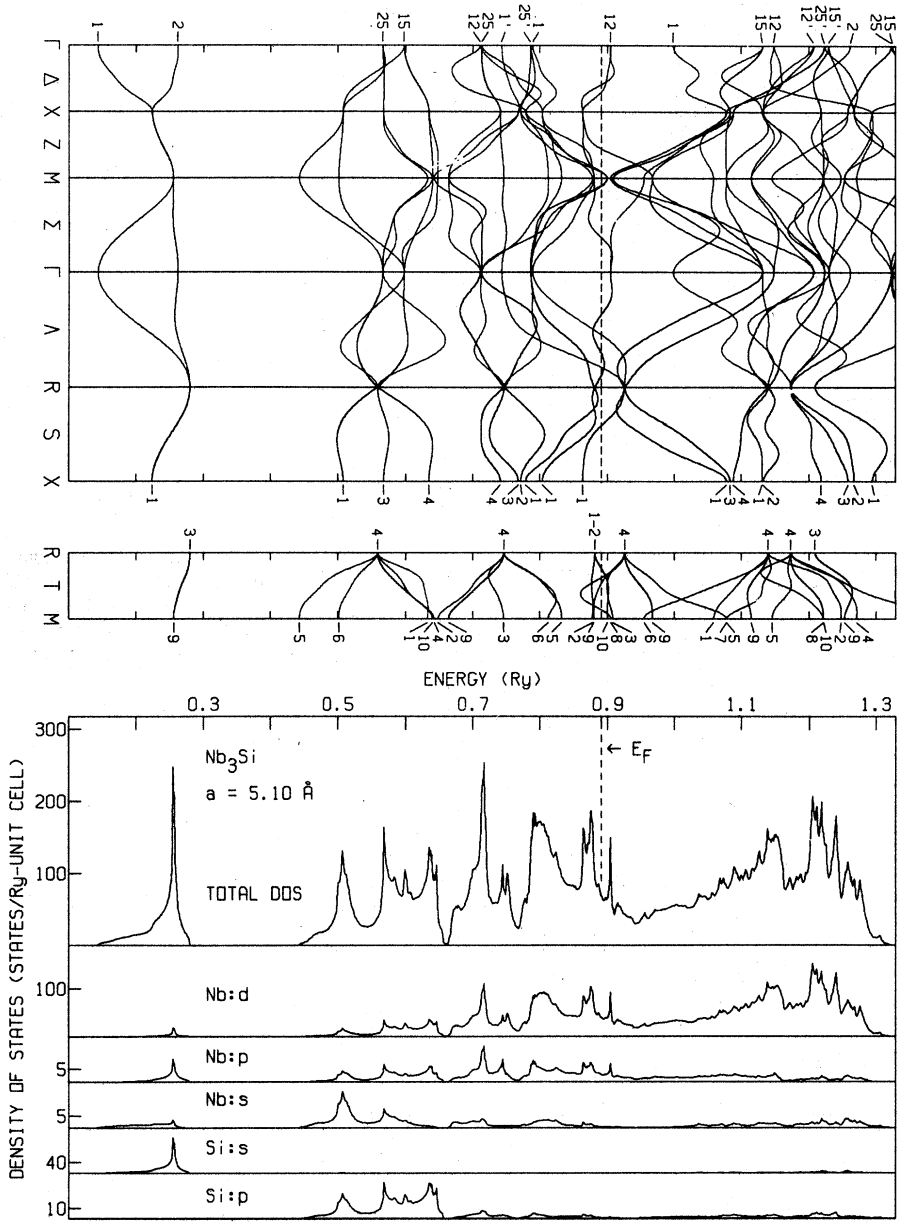

FIG. 11. Self-consistent energy bands and densities of states for Nb_3Si ($a = 5.10$ Å) with the local density approximation exchange.

mi surface areas). In the case of the more complex A-15 materials, where it is of great importance to obtain a good quantitative understanding of the band shapes and $N(E)$ near E_F, it is crucial to determine the sensitivity of the calculated electronic structure to the exchange-correlation approximation.

In the present set of calculations we have performed independent SC calculations for V_3Ga using a Kohn-Sham-Gaspar ($\alpha = \frac{2}{3}$) (Refs. 28 and 29) local exchange potential (both inside and outside the APW spheres), all other calculational procedures remaining the same. Comparing Figs. 3 and 4, it is seen that the energy bands are nearly indistinguishable for the two V_3Ga calculations, including the region near E_F where the extremely flat bands near Γ_{12} persist in both calculations (see Ref. 12 for a comparison of the numerical eigenvalues for the two exchanges). Although there is some quantitative difference in the $N(E)$ fine structure near E_F, the energy *scale* (see Table IV) of the fine structure is nearly the same. We note, however, that our preliminary studies show that the predicted

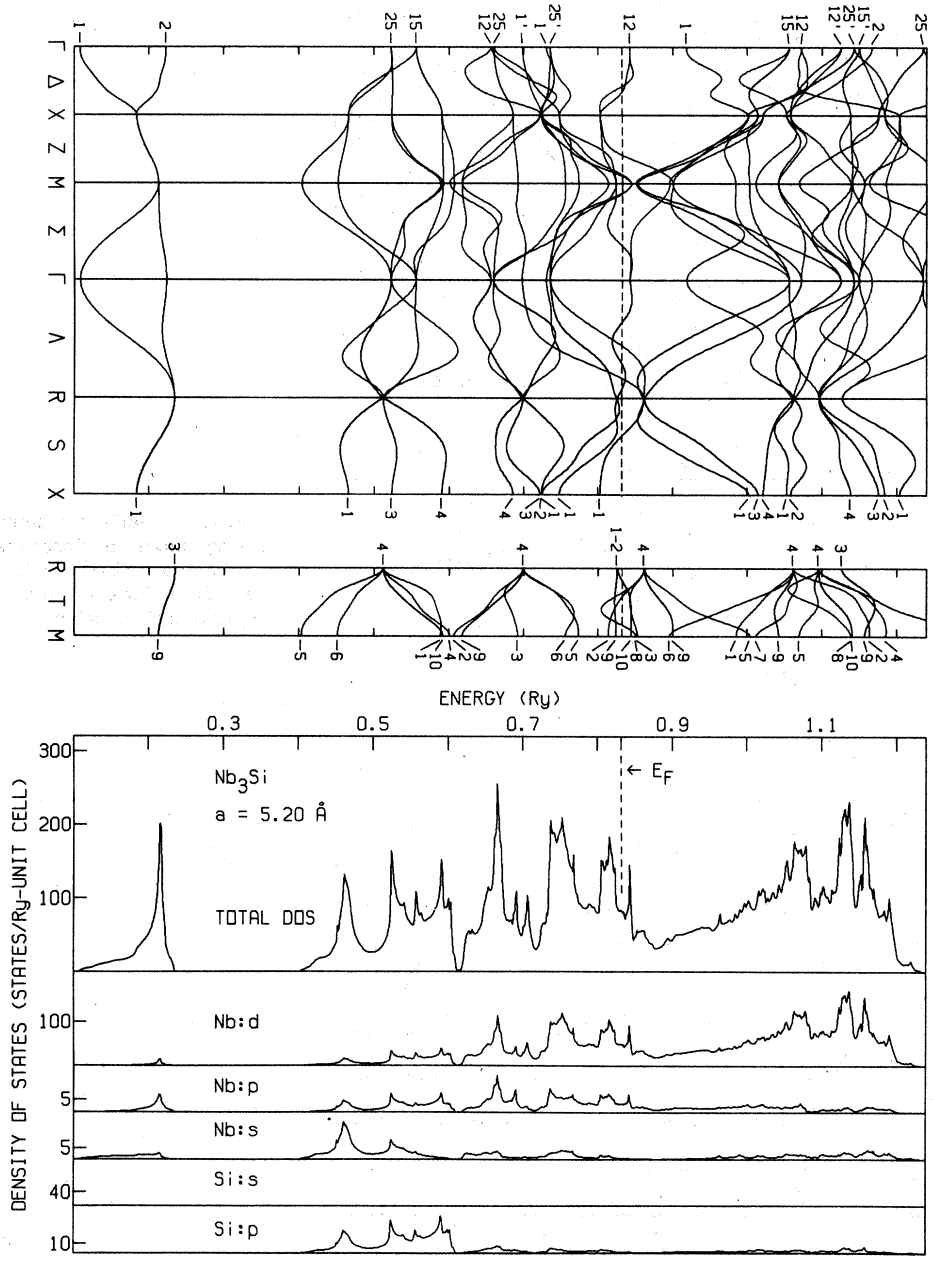

FIG. 12. Self-consistent energy bands and densities of states for Nb_3Si ($a = 5.20$ Å) with the local density approximation exchange.

A-15 Fermi surfaces are considerably more sensitive to the exchange approximation used.

Finally let us note that after the bulk of our calculations were completed we did an $\alpha = \frac{2}{3}$ SC calculation for Nb_3Ge (not shown) to ensure that our conclusions with regard to the superconducting properties of this material were not exchange sensitive. Again the changes in the band structure for this material were minor; and in addition, the $N(E_F)$ values for the two calculations were within ~1% of each other (see further discussion below).

D. Nb_3Ge and Nb_3Si

We now discuss separately our electronic structure results for Nb_3Ge and Nb_3Si. There is special interest in these materials due to the discovery of superconductivity in excess of 23°K (Refs. 41 and

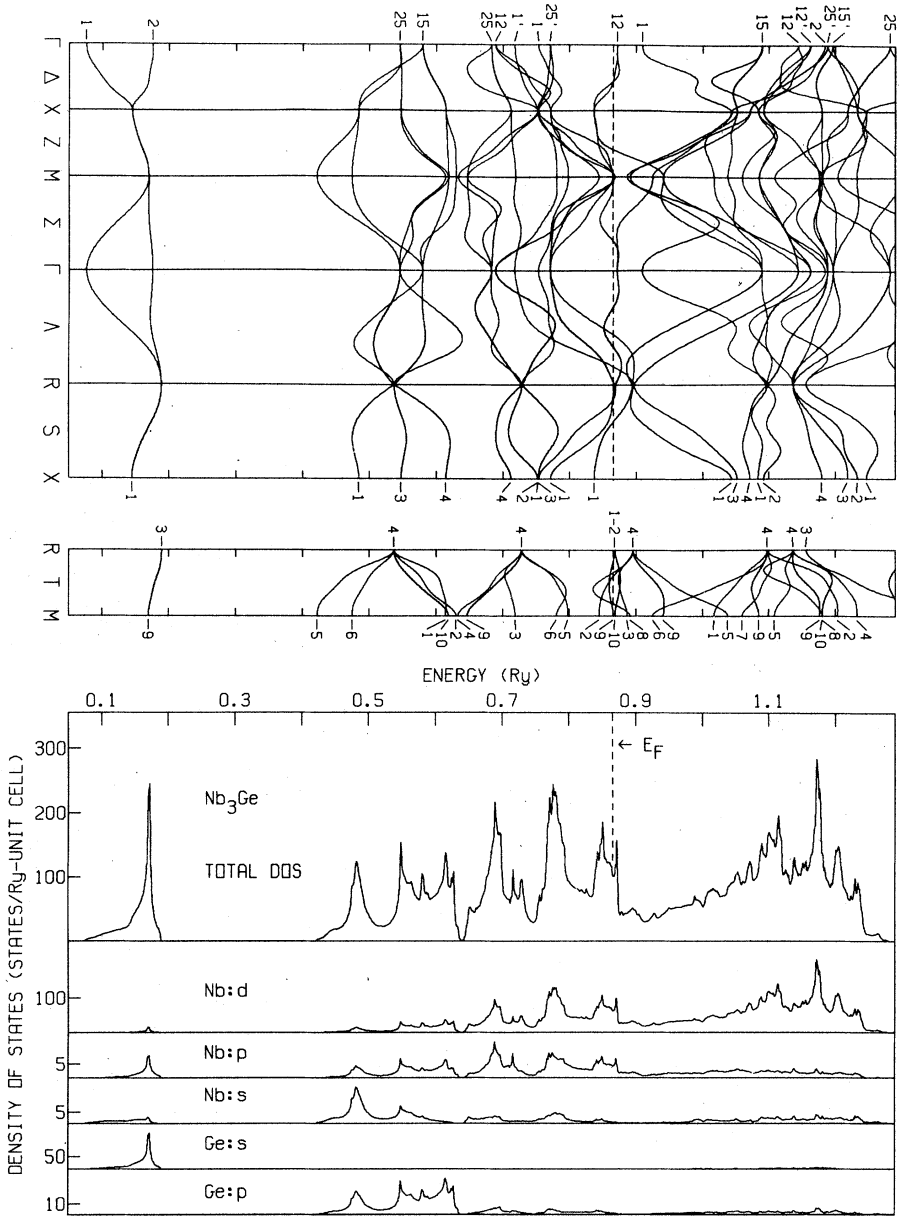

FIG. 13. Self-consistent energy bands and densities of states for Nb_3Ge with the local density approximation exchange.

42) for the former and the prediction of T_c's in excess of 30° K for the latter.[43]

Beginning with Nb_3Ge, we see from Fig. 13 that the position of the Fermi level is atypical of the other high-T_c materials since E_F falls below the Γ_{12}-region flat bands [corresponding to a peak in $N(E)$] by ≈7 mRy. Similarly, E_F falls above the minima in the Σ and Λ branches [again an $N(E)$ maximum] by 14 mRy. From Table III we find that $N(E_F) = 107$ (states/Ry unit cell) for Nb_3Ge, a considerably smaller value than we found in the other high-T_c materials. Detailed calculations, to be described fully in a subsequent paper, shows that the electron-phonon interaction for Nb_3Ge has a value more consistent with that of V_3Ge (relatively low-T_c) than the high-T_c materials (V_3Si, Nb_3Al, etc.), primarily due to the small value of $N(E_F)$.

To make sure that these results for Nb_3Ge are not sensitive to either the lattice constant we used (5.16 Å), or to the exchange potential approximation (LDA), we performed two additional SC cal-

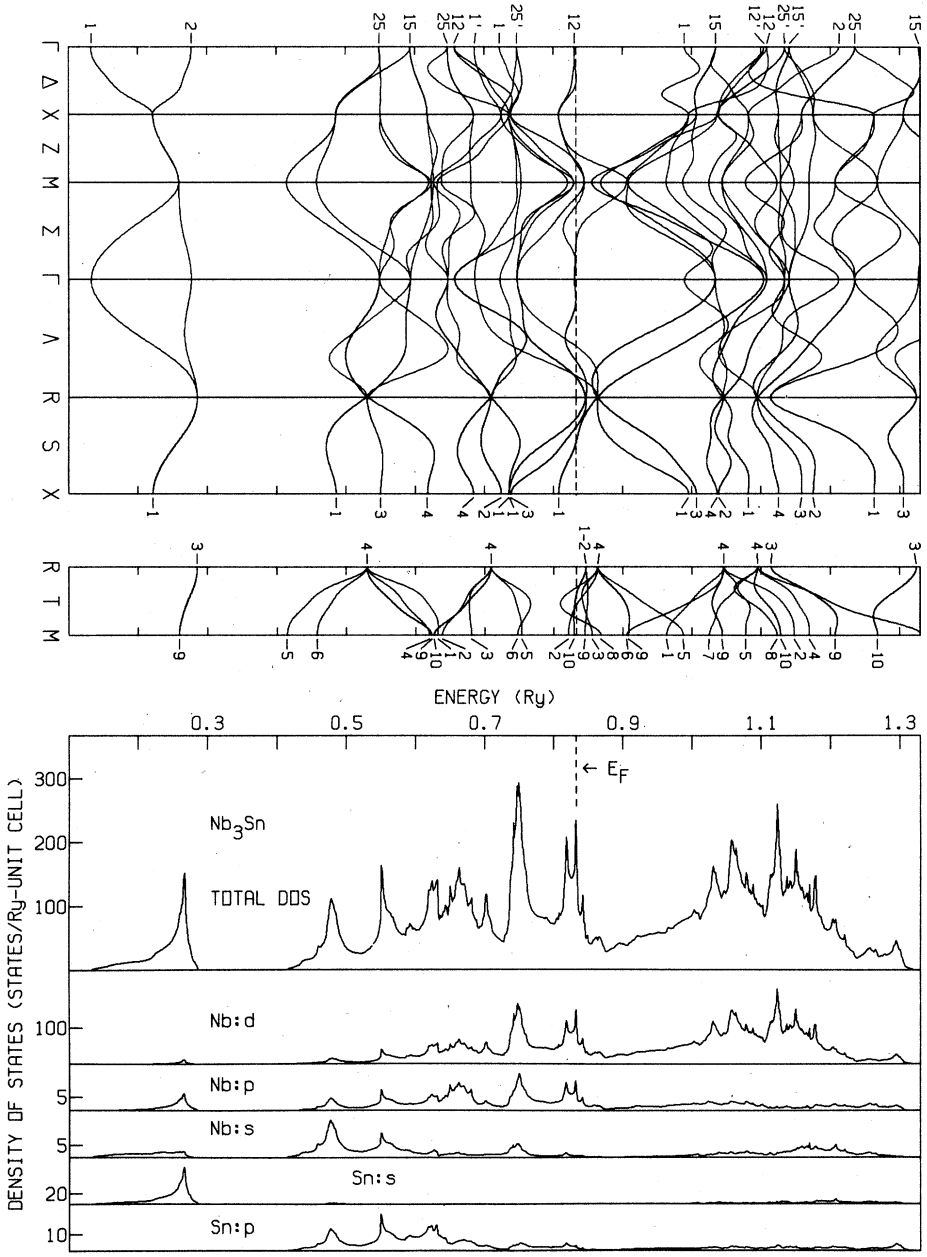

FIG. 14. Self-consistent energy bands and densities of states for Nb_3Sn with the local density approximation exchange.

culations: (a) lattice constant 5.13 Å (closer to the thin-film values[44]), LDA exchange; and (b) lattice constant 5.16 Å, $\alpha = \frac{2}{3}$ exchange. These calculations also show that E_F falls between the two peaks, with states around E_F shifting by ~1 mRy or less from our original calculation. *Within reasonable variations of lattice constant and exchange potential approximations the band structure and N(E) of Nb_3Ge shows minor variations from Fig. 13.*

For Nb_3Si we performed SC-LDA calculations for three different lattice constants: 5.03, 5.10, and 5.20 Å; the first value being that reported by Pan *et al.*,[45] and the latter two spanning the range of *predicted* lattice constants[43,46] for this material which has not been made in an equilibrium bulk configuration. The 5.20 Å value is close to the estimate of the sputtered-film value obtained by Somekh and Evetts.[47] The energy bands and $N(E)$ near E_F are very similar in appearance to Nb_3Ge, with the three $N(E_F)$ values from Table III being

TABLE III. Fermi level E_F, total density of states $N(E_F)$, and the site-angular momentum densities of states $N^l_{A(B)}(E_F)$ for the A-15 materials. All densities of states are in units of (states/Ry unit cell), and are for both spin orientations.

A_3B	E_F (Ry)	$N(E_F)$	N^s_A	N^p_A	N^d_A	N^f_A	N^s_B	N^p_B	N^d_B	N^f_B
V_3Al	0.8186	188.9	0.7818	8.128	130.6	0.7916	0.2970	2.832	2.665	0.1896
V_3Ga (LDA)	0.8265	295.6	0.9533	13.05	211.3	0.9994	0.2280	3.614	2.460	0.2622
V_3Ga ($\alpha=\frac{2}{3}$)	0.8357	237.7	0.8159	10.28	168.7	0.8978	0.2072	3.265	2.287	0.2385
V_3Si	0.8889	200.2	0.4903	7.883	142.6	0.8531	0.2195	1.854	2.954	0.1942
V_3Ge	0.8714	114.7	0.3717	3.508	84.16	0.5851	0.1375	1.242	1.417	0.1436
V_3Sn	0.8031	123.0	0.3344	3.749	92.33	0.6166	0.0883	1.267	1.237	0.2139
Nb_3Al	0.8366	199.2	1.877	8.713	111.2	1.883	0.7157	3.445	5.816	0.2694
Nb_3Ga	0.8507	191.8	1.722	8.979	108.0	1.757	0.5340	4.599	3.481	0.3358
Nb_3Si (5.03 Å)	0.9351	61.42	0.4293	2.588	35.15	0.6248	0.2160	1.094	1.475	0.1266
Nb_3Si (5.10 Å)	0.8905	69.20	0.4323	2.859	39.89	0.6937	0.2116	1.178	1.801	0.1291
Nb_3Si (5.20 Å)	0.8315	83.61	0.4831	3.394	49.46	0.7841	0.2141	1.180	2.121	0.1456
Nb_3Ge	0.8656	106.7	0.5242	4.311	64.19	1.010	0.3427	1.372	1.947	0.1924
Nb_3Sn	0.8329	158.6	0.6629	7.016	98.19	1.378	0.3822	2.151	2.025	0.3560

61, 69, and 84 (states/Ry unit cell), respectively. Our electron-phonon interaction calculations show, as they do for Nb_3Ge, that bulk stoichiometric Nb_3Si does not appear to be a high-T_c material.

Thus we suggest that the high T_c observed for sputtered films of Nb_3Ge must be due to some unusual property of these films (impurities, disorder, or very soft phonons for instance). Somekh and Evetts[47] have obtained enhanced values of T_c for V_3Ge of up to 11°K (versus 6.1°K for the bulk); and values of up to 14°K for sputtered Nb_3Si. There thus seems to be strong evidence, both experimental and theoretical, that there are anomalous properties of sputtered films of A-15 materials that remain to be elucidated. Further quantitative discussion of these points will be made in a subsequent publication.

E. Charge transfer

In Table V we tabulate the electronic charge in the A and B APW spheres (Q_A and Q_B) for the A_3B compounds we have calculated, and also the total charge in the interstitial region Q_{out}. We include results for both the starting overlapping atomic charge-density configurations and the final SC charge density. The last three columns in Table V give the differences Q_i(final) − Q_i(start). The value of Q_{out} is determined by the relation $Q_{out} = 6(Z_A - Q_A) + 2(Z_B - Q_B)$, with Z_A and Z_B being the atomic number of atoms A and B, respectively. The rea-

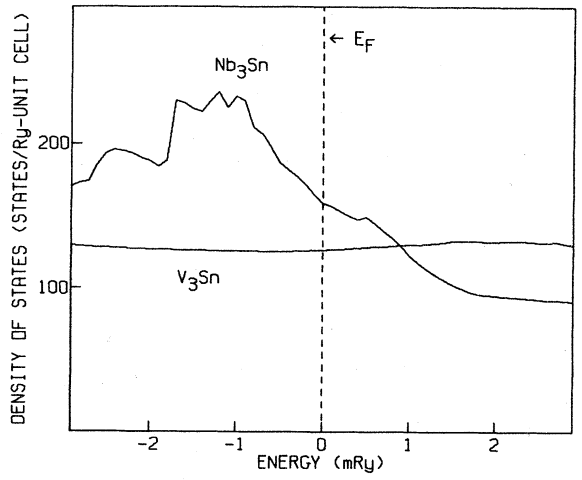

FIG. 15. Total density of states in the vicinity of the Fermi level E_F for V_3Sn and Nb_3Sn.

TABLE IV. Eigenenergies near E_F for several $\vec{k}$ points and irreducible representations for V_3Ga, V_3Si, and Nb_3Sn. The energy values listed are $[E(\vec{k}) - E_F]$ in units of mRy.

$\vec{k}(\pi/4a)$	V_3Ga (LDA)	V_3Ga ($\alpha=\frac{2}{3}$)	V_3Si (LDA)	Nb_3Sn (LDA)
$\Gamma_{12}(000)$	−0.5	0.1	0.6	−2.7
Δ_1 (100)	0.7	1.0	1.5	−1.9
Δ_1 (200)	4.1	4.2	2.8	0.4
Δ_2 (100)	−0.3	0.1	0.0	−2.8
Δ_2 (200)	−1.2	−1.1	−3.3	−5.6
Σ_1 (110)	1.1	1.5	1.2	−1.7
Σ_1 (220)	5.4	5.6	3.9	3.3
Σ_4 (110)	0.5	0.9	0.7	−2.9
Σ_4 (220)	−9.1	−9.4	−15.6	−18.9
Λ_3 (111)	1.3	1.3	0.9	−2.3
Λ_3 (222)	−7.6	−7.6	−13.8	−16.2

TABLE V. Charge-transfer results for the A-15 compounds. Tabulated are the starting (atomic) and final (self-consistent) values of the electronic charges inside (Q_A and Q_B) and outside (Q_{out}) the muffin-tin spheres. The differences between the final and the starting charges are shown in the last three columns.

	Starting			Final			Q(final) − Q(start)		
A_3B	Q_A	Q_B	Q_{out}	Q_A	Q_B	Q_{out}	ΔQ_A	ΔQ_B	ΔQ_{out}
V_3Al	21.51	11.75	11.44	21.21	11.62	13.50	−0.30	−0.13	2.06
V_3Ga	21.48	29.83	11.46	21.22	29.59	13.50	−0.26	−0.24	2.04
V_3Si	21.46	12.56	12.12	21.21	12.29	14.16	−0.25	−0.27	2.04
V_3Ge	21.48	30.54	12.04	21.27	30.19	14.00	−0.21	−0.35	1.96
V_3Sn	21.60	48.06	12.28	21.48	47.41	14.30	−0.12	−0.65	2.02
Nb_3Al	39.26	11.92	12.60	38.54	12.16	16.44	−0.72	+0.24	3.84
Nb_3Ga	39.22	30.04	12.60	38.57	30.19	16.20	−0.65	+0.15	3.60
Nb_3Si (5.03 Å)	39.15	12.78	13.54	38.51	12.94	17.06	−0.64	+0.16	3.52
Nb_3Si (5.10 Å)	39.19	12.80	13.26	38.56	12.95	16.74	−0.63	+0.15	3.48
Nb_3Si (5.20 Å)	39.25	12.84	12.82	38.62	12.97	16.34	−0.63	+0.13	3.52
Nb_3Ge	39.22	30.82	13.04	38.64	30.85	16.46	−0.58	+0.03	3.42
Nb_3Sn	39.34	48.34	13.28	38.82	48.03	17.02	−0.52	−0.31	3.74

der is reminded that the APW sphere radii that we have used are given by $R_A = R_B = \frac{1}{4}a$.

Table V shows that all of the vanadium compounds give up charge to the interstitial region from both the A- and B-atom APW spheres, with the value $\Delta Q_{out} \sim 2$ electrons per unit cell. The situation is different for the niobium compounds, where in all cases each Nb atom gives up 2–4 times more charge to the interstitial region than the vanadium compounds with the same B atom; and the B atoms in Nb_3B gain some charge in all cases except for Sn.

A full charge-density analysis, including the directional properties of the charge density contained within the APW spheres, will be presented in a future publication. At present we can draw some interesting conclusions from the integrated results in Table V. We find that the charge-transfer results for V_3Al, V_3Ga, V_3Si, V_3Ge, and Nb_3Sn are very similar, as is the nature of their energy bands and $N(E)$ near E_F. All of these compounds have flat energy bands around the Γ_{12} state which produce sharp $N(E)$ peaks within a few mRy of E_F. The transfer of substantial amounts of charge to the interstitial region for both the A and B atoms in these compounds probably indicates the presence of covalent A–B bonds in addition to the strong A–A bonds and metallic bonding that is present. This is in qualitative agreement with the charge-density measurements of Staudenmann *et al.* on V_3Si.[48] For V_3Sn, E_F falls well above (~15 mRy) the flat Γ_{12}-derived bands; for this compound ΔQ_{Sn} is negative. We also note that $|\Delta Q_{Sn}| > |\Delta Q_B|$ for each of the other A_3B materials discussed. This suggests that the bonding is substantially different for V_3Sn.

The niobium-based compounds Nb_3Al, Nb_3Ga, Nb_3Si, and Nb_3Ge all have very similar charge-transfer characteristics, with negative ΔQ_{Nb} and positive (small in the case of Ge) ΔQ_B. In all of these compounds E_F falls below the flat region around Γ_{12} by ~15–20 mRy, with the Al and Ga compounds having high values of $N(E_F)$, and the Si and Ge compounds much smaller values. Again the distinction between high and low $N(E_F)$ in these compounds is not discernable from our charge analysis, although it is clear that the charge densities are quite likely to be qualitatively different from the materials with $\Delta Q_B < 0$.

As we have remarked, our charge-transfer analysis is in qualitative agreement with the measurements on V_3Si by Staudenmann *et al.*[48] These authors have applied a less definitive charge-transfer analysis to their V_3Si data following the method of Coppens.[49] In this method a generalized radius is assigned to the V and Si atoms, and charge is associated with either atom depending on the distance of the charge from each atomic position. By inspecting their plot of V or Si versus "radius ratio" they conclude that the appropriate V to Si "radius ratio" is ~1.5, and consequently there is a net charge transfer of 1.8–2.4 electrons per silicon atom *to* the vanadium atoms. Since there is no direct relationship between the generalized Wigner-Seitz radii defined by Staudenmann *et al.*[48] and the APW sphere radii in terms of which we have defined charge transfer, our results are not directly comparable. The method of Coppens[49] associates interstitial charge with either an A or B site in a specific but somewhat arbitrary manner. It is noted, however, that for a "radius ratio" of unity, the results Staudenmann *et al.*[48] suggest essentially

zero charge transfer, a result that is in qualitative agreement with our equal APW sphere radii calculation for V_3Si.

Bongi *et al.*[50,51] have developed a theory of superconductivity in the A_3B compounds based on the notion of charge transfer from the B to the A atoms. As we have discussed, our calculations show no evidence of B- to A-atom charge transfer; in addition, as shown in Table V, there does not seem to be any universality in charge-transfer behavior amongst all of the A_3B compounds for which we have done calculations. In fact we find evidence for charge transfer from Nb to B in several of the Nb_3B compounds.

F. Comparison with previous calculations

There have been a number of previous A-15 band-structure calculations. These include the non-SC APW calculations of Mattheiss[4,5]; the LCAO calculations of Weger, Goldberg, and Barak[2,9-11]; the LMTO calculations of Jarlborg and Arbman[8]; the SC pseudopotential calculations by Ho *et al.*[52]; the non-SC APW calculations by van

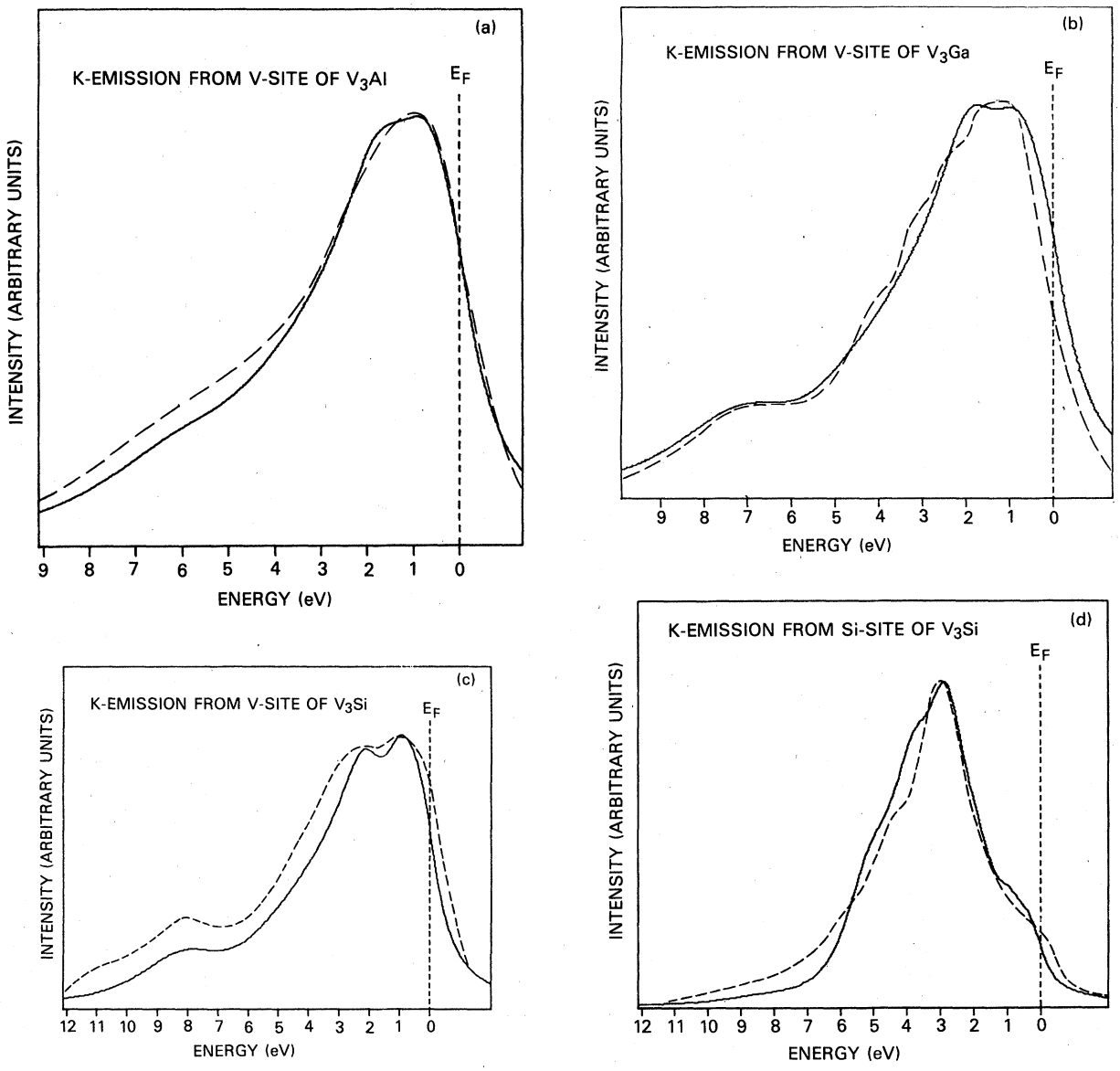

FIG. 16. Calculated (solid curves) and measured (dashed curves) x-ray K-emission spectra of (a) V site of V_3Al, (b) V site of V_3Ga, (c) V site of V_3Si, (d) Si site of V_3Si, (e) V site of V_3Ge, (f) V site of V_3Sn. Experimental spectra are taken from Refs. 59 and 60.

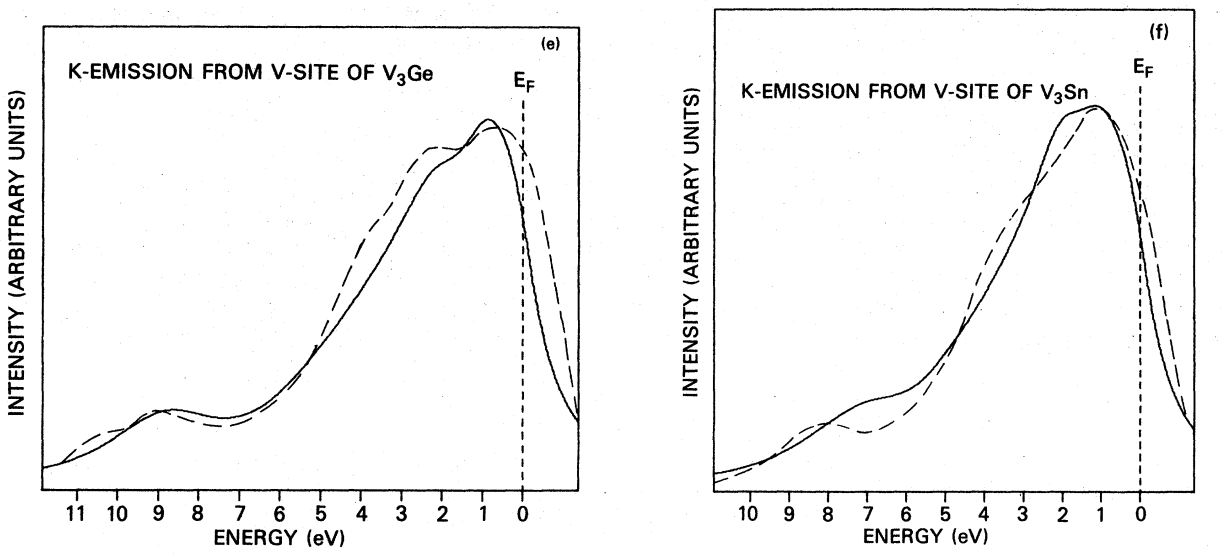

FIG. 16. (*Continued*)

Kessel *et al.*[53]; and the SC-APW calculations by Klein *et al.*[6,7,12]

Mattheiss'[4] 1965 APW results for a number of A-15 materials represented the first accurate electronic-structure results for these compounds. In these calculations he used the non-SC APW method with a convergence accuracy of 10-30 mRy due to the computer limitations at that time. Even so his energy bands for V_3Ga (for E_F at Γ_{12}) are very similar to the ones that we have now obtained with more than an order-of-magnitude better convergence accuracy, although of course there are important differences in the ordering and shape of bands near E_F. Subsequent WMT non-SC calculations by Mattheiss[5] were done for V_3Si, V_3Ge, Nb_3Al, and Nb_3Sn, with ~3 mRy convergence. In these calculations APW eigenvalues were determined at the symmetry points Γ, X, M, and R, and a LCAO interpolation scheme was fit to these values. These LCAO results were used to determine $N(E)$ and to plot the bands for these materials.

Comparing the present SC results with those of Mattheiss[4,5] it is found that the gross features of the energy bands and $N(E)$ curves are similar, with the major difference being the location of the low-energy B-atom s bands with respect to E_F (which are too low in the non-SC results). In addition, there are more detailed differences in band shapes and widths which are due to self-consistency effects and the limited accuracy of the LCAO interpolation procedure. In particular, the LCAO results of Mattheiss fail to reproduce the extremely flat bands that evolve from Γ_{12} in many of these compounds and also the resulting fine structure in $N(E)$. The biggest differences near E_F occur for the compound Nb_3Al, where the energies of some states differ by more than 20 mRy with respect to E_F. This is probably due to the effects of self-consistency, as evidenced by the fact that for Nb_3Al we have found that charge-transfer effects are important, viz., $\Delta Q_{Nb} < 0$ and $\Delta Q_{Al} > 0$ (see Sec. III E).

The recently published LMTO calculations by Jarlborg and Arbman[8] on V_3Si, V_3Ga, and V_3Ge show only density-of-states plots so that a detailed comparison of the band structures, especially details near E_F, is impossible. Jarlborg and Arbman[8] find, as we do, that the gross features of $N(E)$ of these three compounds are very similar, although as we have shown here there are important differences among them on the scale of several mRy around E_F.

The work of Weger, Goldberg, and Barak (WGB),[2,9-11] using an adjusted tight-binding method, predicts band structure and $N(E)$ results for V_3B and Nb_3B compounds which are in considerable disagreement with our work, the previous work of Mattheiss,[4,5] and the calculations of Jarlborg and Arbman.[8] In the WGB calculations, the tight-binding parameters have been adjusted so that the Fermi level coincides with a sharp peak in $N(E)$ arising from flat bands near the Γ_{25}' state. In the present calculations, this Γ_{25}' state consistently falls below E_F by 50–100 mRy for the different compounds. Mattheiss[5] gives a critique of the WGB calculations which we agree with and refer the reader to. We believe that the "empirical" adjust-

ments to the tight-binding parameters made by WGB are not necessary for obtaining sharp structure in $N(E)$ near E_F. Furthermore, the differences in eigenvalues between our results and those of WGB are, we believe, well beyond any corrections to the SC methods that we are using.

IV. X-RAY SPECTRA

A. Theoretical formulation

The K, L, and M x-ray emission spectra to be discussed have been calculated using expressions derived by Goodings and Harris.[54] According to their analysis, the unbroadened x-ray intensity for the K emission spectrum is given by

$$I_0^{K,j}(E) \propto (E - E_c)^3 |M(1s, p, E)|^2 N_j^p(E), \quad (5)$$

while the $L_{2,3}$ (or $M_{2,3}$) spectra involve

$$I_0^{L,j}(E) \propto (E - E_c)^3 [|M(np, s, E)|^2 N_j^s + \tfrac{2}{5} |M(np, d, E)|^2 N_j^d]. \quad (6)$$

In Eqs. (5) and (6), E_c is the core-state energy ($1s$ for the K, $2p$ for the L, and $3p$ for the M spectra),

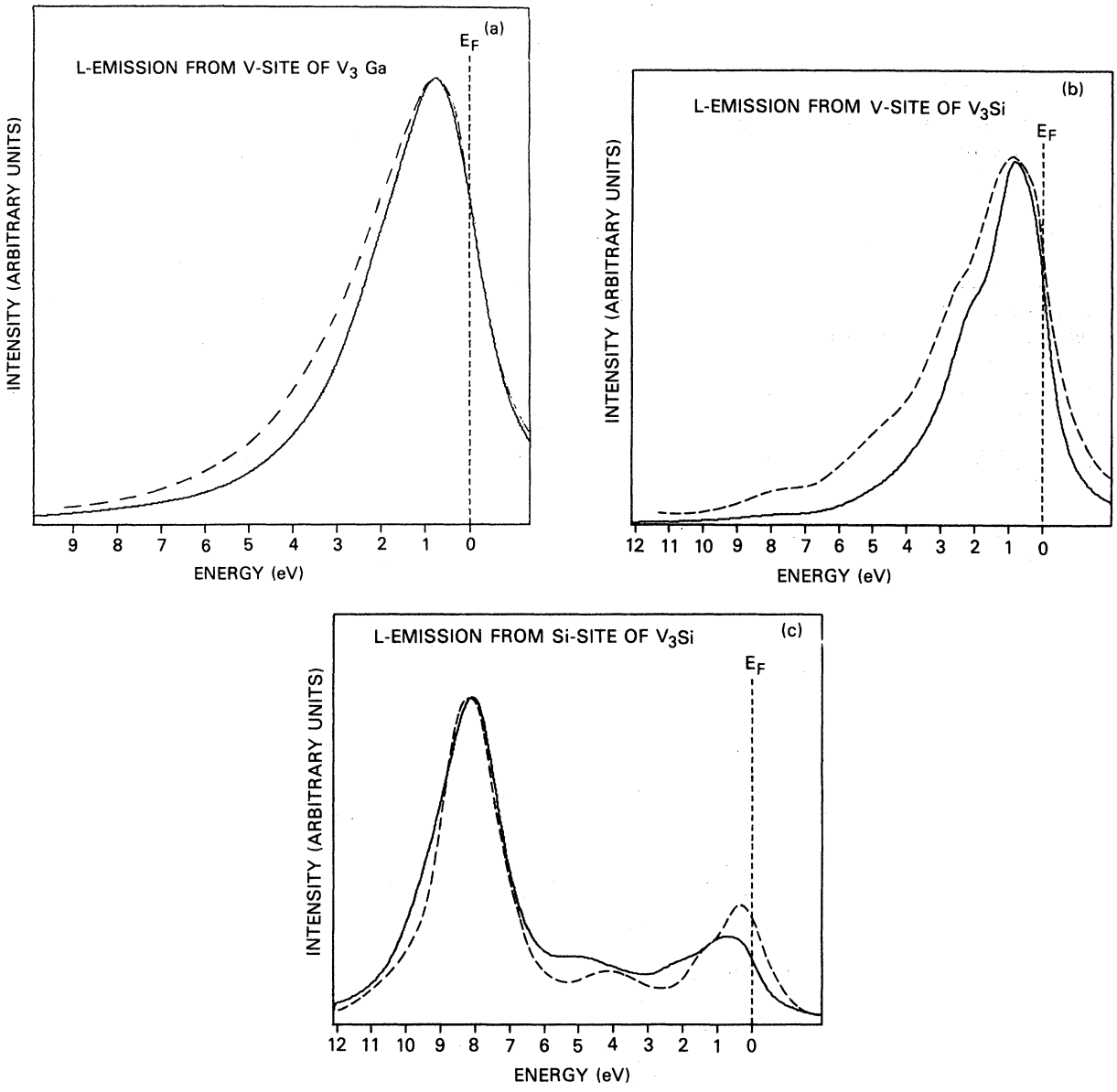

FIG. 17. Calculated (solid curves) and measured (dashed curves) x-ray L-emission spectra of (a) V site of V_3Ga, (b) V site of V_3Si, (c) Si site of V_3Si. Experimental curves are taken from (a) Ref. 61, (b), and (c) Ref. 59.

and N_j^l are the site ($j=A,B$)-angular-momentum (l) decomposed DOS.

The dipole matrix elements are given by

$$M(nl, l\pm 1, E) = \int_0^{R_j} R_{nl}^c(r, E_c) r R_{l\pm 1}^v(r, E) r^2\, dr\,,$$

where R_j is the APW sphere radius and R_{nl}^c and $R_{l\pm 1}^v$ are the core and valence radial wave functions, respectively, both normalized to unity within the APW spheres. The radial wave functions are obtained by solving the wave equation with the crystal potential at the energy E.

To facilitate a comparison with experiment we have broadened I_0 with a Lorentzian function to form

$$I(E) = \int_{E_b}^{E_F} \frac{I_0(E')\gamma(E')\,dE'}{(E-E')^2 + [\frac{1}{2}\gamma(E')]^2} \tag{7}$$

with E_b the bottom of the valence bands.

We have included three separate broadening contributions to the total Lorentzian width $\gamma(E)$, namely,

$$\gamma(E) = \gamma_{\text{spec}} + \gamma_c + \gamma_L(E)\,. \tag{8}$$

Here, γ_{spec} represents the spectrometer resolution, γ_c is the width of the core level, and $\gamma_L(E)$ represents the energy-dependent final-state broadening due to the Auger effect. We have used the experimental values of γ_{spec}, while the values of γ_c were determined from Ref. 55.

We have determined the final-state broadening by the expression

$$\gamma_L(E) = b\int_E^0 N(E')dE' \int_{-|E'-E|}^0 N(E_0) \times N(E_0 + |E'-E|)\,dE_0\,. \tag{9}$$

In Eq. (9), b is a constant and all energies are measured from E_F. This equation accounts for Auger transitions from energy E' filling a hole at energy E, with the excitation of an electron from E_0 to $(E_0 + |E'-E|)$. Further discussion of this formula may be found in Refs. 56 and 57. The only free parameter in Eq. (9) is b, and its value was determined for each spectrum by varying it to obtain a good visual fit to the measured spectrum.

Our XPS calculations were done by broadening the DOS with a Gaussian function. No matrix element, lifetime, or core asymmetry corrections were included in these calculations. The complexities introduced by the variation in photoelectric cross sections for the s, p, and d electrons for the A and B atoms are likely to introduce significant corrections to our simplified calculations.[58] We hope to return to more detailed XPS calculations in future work. In the present work we compare

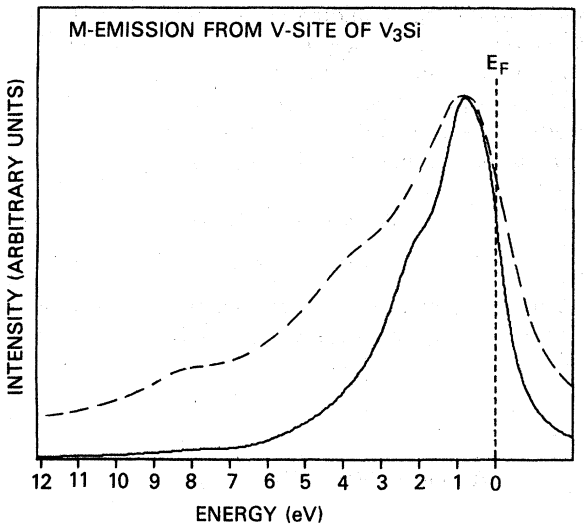

FIG. 18. Calculated (solid curve) and measured (dashed curve) x-ray M-emission spectrum of the V site of V_3Si. Experimental curve is from Ref. 59.

broadened $N(E)$ and also B-atom d DOS $[N_B^d(E)]$ with the available XPS measurements on V_3Si, Nb_3Ge, and Nb_3Sn.

B. X-ray emission results

Figures 16–18 show a comparison of calculated K, L, and M spectra with experimental results.[59-61] Table VI lists the broadening parameters used in these calculations. The agreement between theory and experiment is generally very good for all of the K spectra (Fig. 16), the most serious deviation being for V_3Sn, where the low-energy shoulder (Sn s states) is approximately 1 eV higher in energy than the experimental results. Note that for V_3Ga the calculations are for the local density exchange band structure. The $\alpha = \frac{2}{3}$ band structure gives nearly identical results.

The L spectra shown in Fig. 17 are also in good agreement with experiment, especially so for the Si L spectrum. The experimental L spectra from the vanadium sites in V_3Ga and V_3Si are somewhat

TABLE VI. Broadening parameters used in the x-ray emission spectra calculations for the A-15 compounds [see Eqs. (7)–(9) and Figs. 16–18]. The units are Ry.

	γ_{spec}	γ_c	b
K-vanadium	0.022	0.07	0.1
L-vanadium	0.022	0.09	0.1
M-vanadium	0.022	0.09	0.2
K-silicon	0.022	0.03	0.25
L-silicon	0.022	0.06	0.25

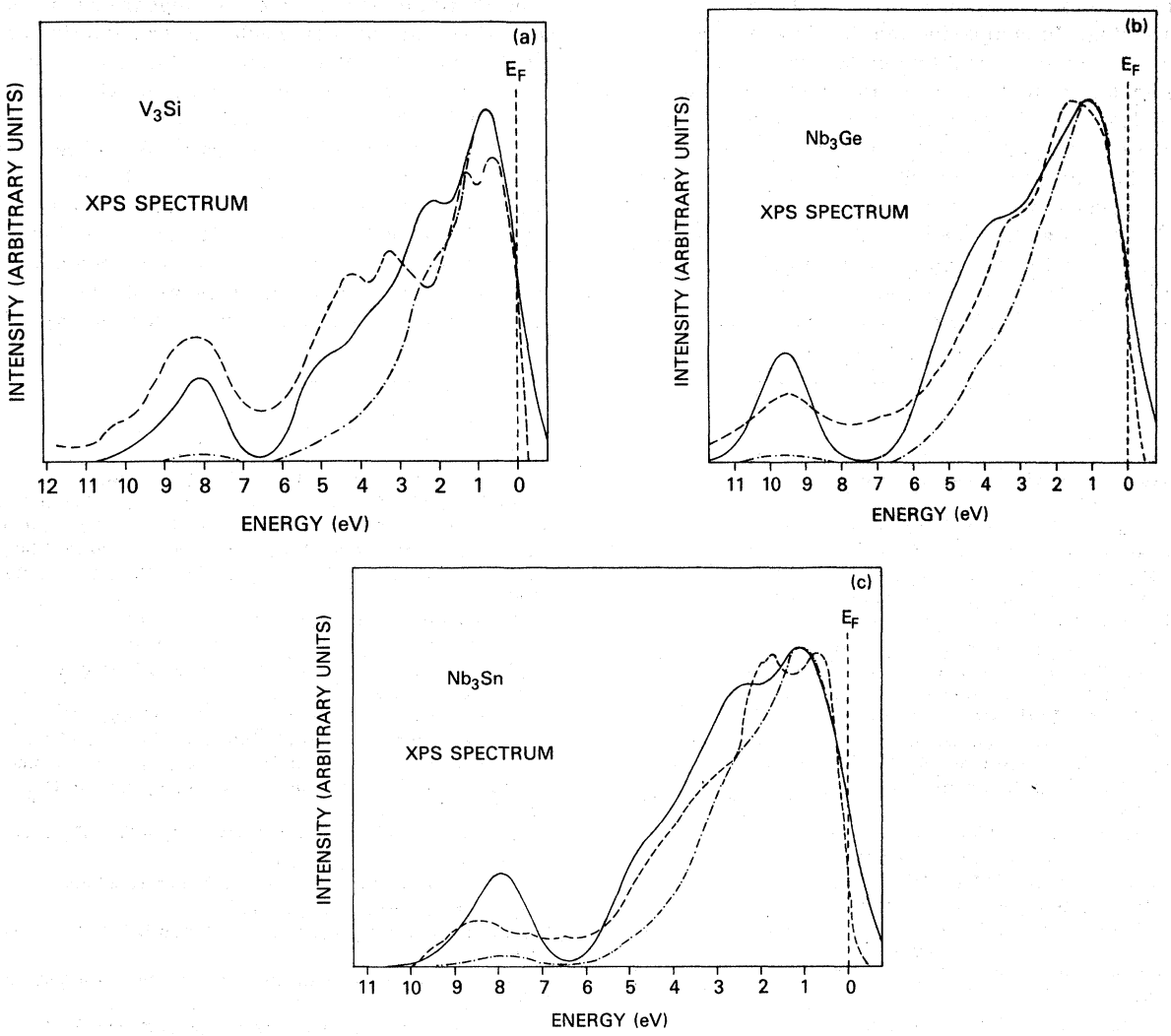

FIG. 19. Calculated and measured XPS spectra of (a) V_3Si, (b) Nb_3Ge, and (c) Nb_3Sn. The solid curves are broadened total DOS and the dot-dashed curves (•—•—) are broadened d-like DOS of V or Nb. The experimental curves are dashed, and are taken from (a) Ref. 62, (b) Ref. 64, and (c) Ref. 65.

broader than the calculated ones, particularly for V_3Si. The calculated vanadium M spectrum shown in Fig. 18 is much too narrow compared to the experimental spectrum, and this is not improved by increasing the broadening parameters. This disagreement for the calculated M spectrum has also been found in calculations for the pure metal vanadium.[57]

Our feeling is that the M spectra are not properly accounted for in the theory due to the neglect of core and/or valence-state relaxation effects beyond the lifetime broadenings that are included. The M-shell energy is close enough to the valence band energies in vanadium, so that the wave functions of the core hole and the valence states may have a significant interaction (and modification) before the x-ray photon is emitted. On the other hand, the K- and L-spectra result from electrons falling into very deep $1s$ or $2p$ core-holes, so that these relaxation effects may be much less important there; and hence the good agreement with experiment for the A-15's and the pure metals also. We are presently studying ways of including these relaxation processes in the x-ray emission theory for elements and compounds.

C. XPS spectra results

Figure 19 shows a comparison of the calculated and measured[62-65] XPS spectra of V_3Si, Nb_3Ge, and Nb_3Sn. The calculations are Gaussian broadened $N(E)$; and V or Nb d-like densities of states $N^d_{V\,(Nb)}(E)$. The experimental curves have not been

corrected for the background inelastic electron scattering. In comparing the theory and experiments two points should be emphasized: (a) due to the neglect of matrix elements, the broadened $N(E)$ includes all of the site-angular-momentum components of the DOS equally weighted and (b) $N^d_{V(Nb)}(E)$ refers to the DOS inside the APW spheres as discussed in Sec. III.

The Gaussian broadening had a 1.2-eV FWHM in all cases. This broadening approximately accounts for the spectrometer broadening (~0.6 eV) and lifetime and core broadening effects. Small changes in the FWHM does not effect the appearance of the theoretical curves very much. An examination of Fig. 19 shows that the broadened $N(E)$ gives a good overall fit to the major features of the XPS measurements. There is some mismatch, especially as to absolute intensities, which is likely due to the neglect of matrix elements. The broadened $N^d_{V(Nb)}(E)$ gives a significantly poorer fit to the experiments, especially for the energy range 3 eV and below E_F. This is the region where the other site-angular-momentum components of $N(E)$ are significant (especially the B-atom s and p states).

[1]L. R. Testardi, in *Physical Acoustics*, edited by W. P. Mason and R. N. Thurston (Academic, New York, 1973), Vol. X.

[2]M. Weger and I. B. Goldberg, in *Solid State Physics*, edited by H. Ehrenreich, F. Seitz, and D. Turnbull (Academic, New York, 1973), Vol. 28.

[3]Yu. A. Izyumov and Z. Z. Kurmaev, Usp. Fiz. Nauk. 113, 193 (1974) [Sov. Phys. Usp. 17, 356 (1974)].

[4]L. F. Mattheiss, Phys. Rev. 138, A112 (1965).

[5]L. F. Mattheiss, Phys. Rev. B 12, 2161 (1975).

[6]B. M. Klein, D. A. Papaconstantopoulos, and L. F. Mattheiss, Bull. Am. Phys. Soc. 20, 297 (1975).

[7]B. M. Klein, D. A. Papaconstantopoulos, and L. L. Boyer, Ferroelectrics 16, 299 (1977).

[8]T. Jarlborg and G. Arbman, J. Phys. F 6, 189 (1976); 9, 1635 (1977).

[9]I. B. Goldberg, J. Phys. C 8, 1159 (1975).

[10]G. Barak, I. B. Goldberg, and M. Weger, J. Phys. Chem. Solids 36, 847 (1975).

[11]M. Weger and G. Barak, Phys. Lett. 48A, 319 (1974).

[12]B. M. Klein, L. L. Boyer, and D. A. Papaconstantopoulos, J. Phys. F 8, 617 (1978).

[13]A. M. Clogston and V. Jaccarino, Phys. Rev. 121, 1357 (1961).

[14]M. Weger, Rev. Mod. Phys. 36, 175 (1964).

[15]J. Labbé and J. Friedel, J. Phys. Radium 27, 153 (1966).

[16]R. W. Cohen, G. D. Cody, and J. J. Halloran, Phys. Rev. Lett. 19, 840 (1967).

[17]L. P. Gor'kov, Pis'ma Zh. Eksp. Teor. Fiz. 17, 525 (1973) [JETP Lett. 17, 379 (1973)]; Zh. Eksp. Teor. Fiz. 65, 1658 (1973) [Sov. Phys. JETP 38, 830 (1974)].

[18]T. K. Lee, J. L. Birman, and S. J. Williamson, Phys. Rev. Lett. 39, 839 (1977).

[19]R. N. Bhatt, Phys. Rev. B 16, 1915 (1977).

[20]L. R. Testardi, Phys. Rev. B 5, 4342 (1972).

[21]L. F. Mattheiss, J. H. Wood, and A. C. Switendick, in *Methods in Computational Physics*, edited by B. Alder, S. Fernbach, and M. Rotenberg (Academic, New York, 1968), Vol. 8.

[22]D. A. Liberman, D. T. Cromer, and J. T. Waber, Comput. Phys. Commun. 2, 107 (1971).

[23]S. Asano and J. Yamashita, J. Phys. Soc. Jpn. 30, 667 (1971). In the notation of this reference, the Ewald constants for the A-15 structure are $M_{AA} = -5.055\,922/a$; $M_{BB} = -3.639\,233/a$, $M_{AB} = -0.707\,8015/a$, $M_{BA} = 3M_{AB}$, with a being the cubic lattice constant.

[24]D. A. Papaconstantopoulos and W. R. Slaughter, Comput. Phys. Commun. 7, 207 (1974); 13, 225 (1977).

[25]D. D. Koelling and B. N. Harmon, J. Phys. C 10, 3107 (1977).

[26]L. F. Mattheiss, Phys. Rev. 151, 450 (1966).

[27]L. Hedin and B. I. Lundqvist, J. Phys. C 4, 2064 (1971).

[28]W. Kohn and L. J. Sham, Phys. Rev. 140, A1133 (1965).

[29]R. Gaspar, Acta Phys. Acad. Sci. Hung. 3, 263 (1954).

[30]H. Schlosser and P. M. Marcus, Phys. Rev. 131, 2529 (1963).

[31]P. D. DeCicco, Phys. Rev. 153, 931 (1967).

[32]W. E. Rudge, Phys. Rev. 181, 1024 (1969).

[33]D. D. Koelling, A. J. Freeman, and F. M. Mueller, Phys. Rev. B 1, 1318 (1970).

[34]D. D. Koelling, Phys. Rev. 188, 1049 (1969).

[35]L. F. Mattheiss, MIT Solid State and Molecular Theory Group Quarterly Progress Report No. 51, 1964 (unpublished), p. 54; W. Gorzkowski, Phys. Status Solidi 3 910 (1963).

[36]L. L. Boyer, Bull. Am. Phys. Soc. 23, 433 (1978); and Phys. Rev. B (to be published).

[37]G. Lehmann, P. Rennert, M. Taut, and H. Wonn, Phys. Status Solidi 37, K27 (1970).

[38]G. Lehmann and M. Taut, Phys. Status Solidi 54, 469 (1972).

[39]O. Jepsen and O. K. Andersen, Solid State Commun. 9, 1763 (1971).

[40]L. L. Boyer, D. A. Papaconstantopoulos, and B. M. Klein, Phys. Rev. 15, 3685 (1977).

[41]J. R. Gavaler, Appl. Phys. Lett. 23, 480 (1973).

[42]L. R. Testardi, J. H. Wernick, and W. A. Royer, Solid State Commun. 15, 1 (1974).

[43]See, for instance, S. Geller, Appl. Phys. 7, 321 (1975).

[44]P. H. Schmidt, E. G. Spencer, D. C. Joy, and J. M. Rowell, in *Superconductivity in d- and f-Band Metals*, edited by D. H. Douglass (Plenum, New York, 1976).

[45]V. M. Pan, V. P. Alekseevskii, A. G. Popov, Yu. I. Belekskii, L. M. Yupko, and V. V. Yarosh, Pis'ma Zh. Eksp. Teor. Fiz. 21, 494 (1975) [JETP Lett. 21, 228 (1975)].

[46]G. R. Johnson and D. H. Douglass, J. Low Temp. Phys. 14, 575 (1973).

[47]R. E. Somekh and J. E. Evetts, Solid State Commun. 24, 733 (1977).

[48]J. L. Staudenmann, P. Coppens, and J. Muller, Solid State Commun. 19, 29 (1976).

[49]P. Coppens, Phys. Rev. Lett. 35, 98 (1975).

[50]G. Bongi, Ø. Fischer, and H. Jones, J. Phys. F 4, L259 (1974).

[51]G. H. Bongi, J. Phys. F 6, 1535 (1976).

[52]K. H. Ho, W. E. Pickett and M. L. Cohen, Phys. Rev. Lett 41, 580 (1978).

[53]A. T. van Kessel, H. W. Myron, and F. M. Mueller, Phys. Rev. Lett. 41, 181 (1978); 41, 520 (E) (1978); Bull. Am. Phys. Soc. 23, 416 (1978).
[54]D. A. Goodings and R. Harris, J. Phys. C 2, 1808 (1969).
[55]K. D. Sevier, *Low Energy Electron Spectroscopy* (Wiley, New York, 1972), Chap. 6, p. 220.
[56]D. J. Nagel, Ph.D. thesis (University of Maryland, 1977) (unpublished).
[57]D. A. Papaconstantopoulos, D. J. Nagel, and C. Jones-Bjorklund (unpublished).
[58]See, for instance, R. J. Baird, L. F. Wagner, and C. S. Fadley, Phys. Rev. Lett. 37, 111 (1976); P. S. Wehner, J. S. Stöhr, G. Apai, F. R. McFeely, and D. A. Shirley, *ibid.* 38, 169 (1977); H. Höchst, P. Steiner, and S. Hüfner, J. Phys. F 7, L309 (1977).
[59]E. Z. Kurmaev, V. P. Belash, S. A. Nemnovov, and A. S. Shulakov, Phys. Status Solidi 61, 365 (1974).
[60]E. Z. Kurmaev, S. A. Nemnonov, V. P. Belash, and Yu. V. Yefimov, Fiz. Met. Metalloved. 33, 578 (1972) [Phys. Met. Metallog. 33, 118 (1972)].
[61]E. Z. Kurmaev, V. P. Belash, S. A. Nemnonov, I. A. Brytov, N. S. Vorob'yeva, and V. I. Sokolov, Fiz. Met. Metalloved. 31, 753 (1971) [Phys. Met. Metallog. 31, 79 (1971)].
[62]J. Riley, J. Azoulay, and L. Ley, Solid State Commun. 19, 993 (1976).
[63]P. O. Nilsson, I. Curelaru, and T. Jarlborg, Phys. Status Solidi B 79, 277 (1977).
[64]R. A. Pollak, C. C. Tsuei, and R. W. Johnson, Solid State Commun. 23, 879 (1977).
[65]H. Höchst, S. Hüfner, and A. Goldmann, Solid State Commun. 19, 899 (1976).